Acta Mech (2007)
DOI 10.1007/s00707-007-0507-z
Printed in The Netherlands

Acta Mechanica

Couette flow in channels with wavy walls

A. E. Malevich[1], V. V. Mityushev[2], P. M. Adler[3]

[1] BSU, Minsk, Belarus
[2] Department of Mathematics, Pedagogical Academy, Krakow, Poland
[3] UPMC-Sisyphe, Paris Cedex 05, France

Received 22 February 2007; Accepted 20 August 2007; Published online 30 October 2007

Summary. Three–dimensional Couette flows enclosed by a plane and by a wavy wall are addressed; the wave amplitude is proportional to the mean clearance of the channel multiplied by a small dimensionless parameter ε. A perturbation expansion in terms of the powers of ε of the full steady Navier–Stokes equations yields a cascade of boundary value problems which are solved at each step in closed form. The supremum value of ε for which the expansion converges, is determined as a function of the Reynolds number $\mathcal{R}e$. The analytical-numerical algorithm is applied to compute the velocity in the channel to $O(\varepsilon^4)$. Even in the first order approximation $O(\varepsilon)$, new results are obtained which complement the triple deck theory and its modifications. In particular, the incipient separation–detachment is discussed using the Prandtl-Schlichting criterion of starting eddies. The value ε_e for which eddies start in the channel, is analytically deduced as a function of $\mathcal{R}e$ as well as analytical formulas for the coordinates of the separation points. These analytical formulas show that ε_e in 3D channels is always less than ε_e in 2D channels. For non-smooth channels, a criterion of infinitesimally small ε_e is deduced. The critical value of ε up to which bifurcation of the solutions can occur is estimated.

1 Introduction

This paper is devoted to the theoretical study of the stationary Couette flow through periodic curvilinear channels. This problem is of fundamental interest for fluids mechanics.

The structure of the stationary flow depends on the geometry of the channel which could be very complicated, on the external forces and on the Reynolds number $\mathcal{R}e$. The vertical coordinates of the upper and lower walls (denoted by $z^{\pm}$) are given by

$$z^{+} = b\Big[1 + \varepsilon T\Big(\frac{\pi}{L}x, \frac{\pi}{L}y\Big)\Big], \quad z^{-} = b\varepsilon B\Big(\frac{\pi}{L}x, \frac{\pi}{L}y\Big), \tag{1.1}$$

where x and y are the coordinates in the horizontal plane. ε is assumed to be a non-negative small dimensionless parameter. The functions $T(x, y)$ and $B(x, y)$ model the oscillations of the walls with the amplitude $b\varepsilon$; $T(x, y)$ and $B(x, y)$ stand for top and bottom, respectively; b is the width of the plane channel ($\varepsilon = 0$); L is the half–period of the channel along the x- and y- directions. The upper surface moves with the velocity U_o.

Correspondence: Pierre M. Adler, UPMC-Sisyphe, tour 56, place Jussieu, 75252 Paris Cedex 05, France
e-mail: adler@ipgp.jussieu.fr

We are interested in the analytical dependence of the velocity field in the channel on ε, T, B and $\mathcal{R}e$. The theoretical results which were already obtained, should be summarized. First, in the Stokes approximation ($\mathcal{R}e = 0$), the circular and plane Couette flow past a wavy wall were considered by Munson et al. [17] by using the stream function. The velocity was determined up to $O(\varepsilon^4)$ by a perturbation expansion in the channel bounded by the cylinders defined by the radial coordinates R (moving) and R + b sin $p\theta$ (rest) where b is the amplitude of the waves and p is the wave number. Similar solutions for the plane Couette flow past a wavy wall were also obtained. It was shown that the streamlines follow the wavy wall for small ε. The existence of eddies was demonstrated by calculating the longitudinal velocity near the bottom of the wavy wall. Munson et al. [17] calculated the critical value ε_e of the start of an eddy. Various problems for two-dimensional channels were studied by Scholle et al. [24]–[27] (see also papers cited therein). In particular, Scholle [25] applied the complex potential method to the plane Couette flow for a channel bounded by the surfaces $z = b$, $z = -\varepsilon b \cos\frac{\pi}{L}x$. Scholle's solution is based on Cauchy's integral representation of complex potentials and on the Fourier series for the unknown integral densities. As a result, an infinite linear algebraic system was obtained and numerically solved by the truncation method. Sisavath et al. [42] studied the lubrication approximation for a sinusoidal wall. They obtained a simple expression relating the effective hydraulic aperture of the channel to the mean aperture and to the amplitude and wavelength of the wall profile.

Stokes flow in wavy three-dimensional channels was systematically investigated in [16] for arbitrary wall shapes as an extension to the seminal paper of [19]. An analytical-numerical algorithm proposed in [16] yields efficient formulas for velocities and permeability. These formulas include ε in symbolic form. When ε increases, the Poiseuille flow ($\varepsilon = 0$) is disturbed and eddies can arise above a critical value ε_e which was exactly computed for various channels in [16]. The papers [24]–[27], [17], [16] contain many other interesting results and an extensive literature devoted to Stokes flow.

Consider now the role of inertia in such flows. For a fixed geometry, an important threshold parameter is the value of the critical Reynolds number $\mathcal{R}e = \mathcal{R}e_e$, for which eddies start in the channel. The Poiseuille flow with non-zero Reynolds number $\mathcal{R}e$ was studied by Zhou et al. [45] for three 2D channels when one of the walls is sinusoidal, arched or triangular; the second wall is a plane. An asymptotic expansion up to $O(\varepsilon^1)$ and a finite volume method were used. $\mathcal{R}e_e$ was numerically estimated for various ε and wave numbers; a heuristic relation between $\mathcal{R}e_e$ and ε was suggested. For instance, for the sinusoidal wall $z = \varepsilon \sin\frac{\pi}{L}x$, $\mathcal{R}e_e$ was empirically deduced as

$$\mathcal{R}e_e = \frac{3.18}{\pi} L^2 \varepsilon^{-2.5}. \tag{1.2}$$

Lenweit and Awerbuch [14] studied numerically and experimentally the conditions under which eddies arise in symmetric sinusoidal 2D channels bounded by the walls $z = \pm z_0 + \varepsilon \cos\frac{\pi}{L}x$ for moderate Reynolds numbers. The authors showed that the increase of the separation region with increasing $\mathcal{R}e$ is sensitive to the geometrical parameters. The locations of the separation points for fixed geometries and fixed $\mathcal{R}e$ were studied numerically.

Experimental studies were made by Stephanoff at all [38], Zhou et al. [45], Leneueit [14], Lagrée at all [11] and many others as cited in these papers.

For larger Reynolds numbers, the triple deck theory was applied to study viscous flow in boundary layers [20], [29]–[33], [39]–[41]. An extensive review of the stationary problems with historical notes on the triple deck theory is made by Sobey [37]. The asymptotic analysis when $\mathcal{R}e$ tends to infinity, was performed up to $O(\varepsilon^1)$ and $O(b/L)$ in our notations. According to the triple deck theory, the velocity was rigorously estimated at the lower and upper walls for Poiseuille flows. Though the average width b of the channel is small, the flow was not always laminar, especially for larger $\mathcal{R}e$.

The critical Reynolds number for separation was estimated for asymmetric ($T(x',\, y') = 0$) and vertically symmetric ($T(x',\, y') = -B(x',\, y')$) 2D channels under the additional assumption that $\mathcal{R}e^{1/7}b/L$ is suitably small as follows

$$\varepsilon \sim \left(\frac{L}{b\mathcal{R}e}\right)^{1/3}. \tag{1.3}$$

The value of ε deduced from (1.3) is small, since $\left(\frac{L}{b\mathcal{R}e}\right)^{1/3}$ can be small simultaneously with $\mathcal{R}e^{1/7}b/L$. The estimation (1.3) yields (compare to the empirical formula (1.2))

$$\mathcal{R}e_e = c\frac{L}{b}\varepsilon^{-3}, \tag{1.4}$$

where the constant c depends on the channel shape. Sobey [37] computed c for various channels. The location $x_e = x$ of the separation point was estimated [37, p. 274] in the channel as

$$x_e = -0.49\frac{L}{\pi}\mathcal{R}e^{1/7} + d, \tag{1.5}$$

where d is a suitable constant calculated numerically.

Lagrée et al. [10] deduced the reduced Navier–Stokes equations which are equivalent to the Prandtl equations with different boundary conditions. A connection was established between their equations and the other asymptotic descriptions including the triple deck theory discussed above. The reduced Navier–Stokes equations were also applied to evolution problems [9]–[12].

The interactive boundary layer theory based on the reduced Navier–Stokes equations is a powerful method to study channel flows ([20], [29]–[33], [39]–[41]). In particular, the important formulas (1.3)–(1.4) for the critical Reynolds number and (1.5) for the separation point were rigorously deduced for $\mathcal{R}e \to +\infty$. Together with empirical formulas like (1.2), they provide qualitative and quantitative estimations of $\mathcal{R}e_e$ and x_e. Assuming that $\mathcal{R}e \to +\infty$, the previous authors made additional restrictions like $b \ll L$ and $\varepsilon \ll 1$. For the unsteady separation and the onset of transition, the reader is referred to [5], [21], [44].

In the present paper, the full Navier–Stokes equations are treated in 3D curvilinear channels considering ε as a small parameter without any restriction on the shape of the bottom wall. The method applied to the linear Stokes equations in [16] which is based on the use of power series in ε, is extended. Though the boundary layer theory [22] and its sophisticated modifications ([20], [29]–[35], [37]) are not directly used, the method is applied to the same questions such as the incipient separation–detachment, with the same criteria such as the Prandtl-Schlichting criterion of starting eddies. The main advantage of the proposed method is that the flow is analytically described in terms of the geometry of the channels for any Reynolds numbers in contrast with the triple deck theory. This allows us to correct the flow characteristics in curvilinear channels derived by the previous authors, and to extend them. Among other results, new features relative to steady flow are presented, such as a criterion for the existence of an eddy in channels with non-smooth bottoms and flow sensitivity to 2D and 3D perturbations.

This paper is organized as follows. In Sect. 2, we consider the Couette problem for 3D channel bounded by the walls

$$z = b, \quad z = \varepsilon b B\Big(\frac{\pi}{L}x,\, \frac{\pi}{L}y\Big), \tag{1.6}$$

where $B(x',\, y')$ is an arbitrary periodic function. A perturbation analysis in ε yields a cascade of boundary value problems. Only the zero-th approximation corresponds to a trivial non-linear problem, since it is the Couette problem for a straight channel. The higher approximations in ε yield linear boundary value problems where $\mathcal{R}e$ enters as a parameter.

In Sect. 3, the problem is reduced to a non-local problem for a set of ordinary differential equations. A general algorithm for this problem is presented in Sect. 4.1 without any restriction on geometry, i.e., on $B(x', y')$. It is only assumed that $B(x', y')$ can be expanded as a double Fourier series which is uniformly convergent almost everywhere. Sect. 5 is devoted to the study of the first order approximation for 2D channels. The velocity, the critical ε of onset of eddies, the separation point are calculated analytically to the first order in ε. In particular, a criterion for eddies is deduced for channels with non-smooth walls. Section 6 is devoted to the first order approximation for the velocity in 3D channels. In Sect. 7, boundary layer separation in 3D channels is discussed and a theorem is proved which compares separation in 3D and 2D channels. Applications of higher order expansions in ε are presented in Sect. 8 for a sinusoidal channel. Special attention is paid to the asymptotics when $\mathcal{R}e$ tends to infinity. A general formula for the force acting on the upper wall is deduced up to $O(\varepsilon^4)$. Symbolic–numerical computations are performed up to $O(\varepsilon^5)$ in a sinusoidal channel. Sect. 9 is devoted to the bifurcation analysis of the problem. It is established that bifurcation can arise only for $\varepsilon > \varepsilon_c$, where ε_c is the critical value up to which the algorithm converges. The results are summarized and compared with other works in Sect. 10. Appendix A contains the estimation of ε_c.

2 Statement of the problem

Let us consider an arbitrary 3D dimensional channel which is spatially periodic along the x- and y-directions with periods $2L$; the channel is bounded by the walls $z = b$ and $z = b\varepsilon B\left(\frac{\pi}{L}x, \frac{\pi}{L}y\right)$ and represented by the cell displayed in Fig. 1,

$$Q = \left\{\{x, y, z\} \in \mathbb{R}^3 : -L < x,\ y < L, b\varepsilon B\left(\frac{\pi}{L}x,\ \frac{\pi}{L}y\right) < z < b\right\}, \tag{2.1}$$

where $B(x, y)$ is a 2π-periodic infinitely differentiable function for which

$$\int_{-\pi}^{\pi}\int_{-\pi}^{\pi} B(x, y)dxdy = 0. \tag{2.2}$$

Let $\mathbf{u} = \mathbf{u}(x, y, z)$ be the velocity vector, $p(x, y, z)$ the pressure, μ the fluid viscosity, and ρ its constant density. The flow is governed by the Navier–Stokes equations

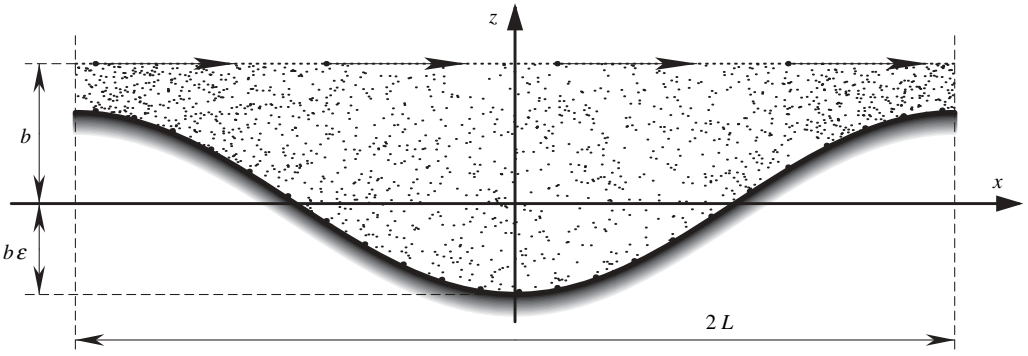

Fig. 1. Schematic diagram and the geometric notations. The axes are denoted by x, y and z; the transversal coordinate is y. The average aperture is equal to b; the amplitude of the bottom is equal to $b\varepsilon$

$$\mu\nabla^2\mathbf{u} = \nabla p + \rho(\mathbf{u}\cdot\nabla)\mathbf{u}, \quad \nabla\cdot\mathbf{u} = 0, \tag{2.3}$$

which are supplemented by the boundary conditions for a Couette flow

$$\mathbf{u}(x,y,b) = U_0(1,0,0), \quad \mathbf{u}\Big[x,y,b\varepsilon B\Big(\frac{\pi}{L}x,\frac{\pi}{L}y\Big)\Big] = \mathbf{0}, \tag{2.4}$$

where U_0 is a positive constant. For convenience, dimensionless quantities indicated by primes are introduced in the three next equations:

$$(x',y',z') = \frac{L}{\pi}(x',y',z'), \quad b = \frac{L}{\pi}b', \quad \mathbf{u} = U_0\mathbf{u}', \quad p = \frac{\pi U_0\mu}{L}p'. \tag{2.5}$$

Then, Eqs. (2.3) take the following dimensionless form:

$$\nabla'^2\mathbf{u}' = \nabla' p' + \mathcal{R}e(\mathbf{u}'\cdot\nabla')\mathbf{u}', \quad \nabla'\cdot\mathbf{u}' = 0, \tag{2.6}$$

where $\mathcal{R}e = \frac{\rho U_0 L}{\pi\mu}$ is the Reynolds number. The boundary conditions (2.4) become

$$\mathbf{u}'(x',y',b') = (1,0,0), \quad \mathbf{u}'(x',y',b'\varepsilon B(x',y')) = \mathbf{0}. \tag{2.7}$$

For brevity, the primes for dimensionless values are omitted in the rest of this paper. A solution to Eqs. (2.6)–(2.7) is looked for as an expansion in ε

$$\mathbf{u}(x,y,z) = \sum_{n=0}^{\infty}\mathbf{u}_n(x,y,z)\varepsilon^n, \quad p(x,y,z) = \sum_{n=0}^{\infty}p_n(x,y,z)\varepsilon^n. \tag{2.8}$$

where $\mathbf{u}_0$ and p_0 satisfy the zero-th problem, i.e., the Eqs. (2.6) in the channel $0 \le z \le b$ with the following boundary conditions:

$$\mathbf{u}_0(x,y,b) = (1,0,0), \quad \mathbf{u}_0(x,y,0) = \mathbf{0}. \tag{2.9}$$

This is the classical Couette problem [22], [23] for a plane channel whose solution is

$$u_0(x,y,z) = \frac{z}{b}, \quad v_0(x,y,z) = 0, \quad w_0(x,y,z) = 0, \quad p_0(x,y,z) = \text{constant}, \tag{2.10}$$

where $\mathbf{u}_n(x, y, z) = [\, u_n(x, y, z), v_n(x, y, z), w_n(x, y, z)]$, $n = 0,1, \ldots$ Substitute Eqs. (2.10) into (2.8), and then into (2.6). Further, select coefficients with the same powers in ε. The cascade of equations in the layer $0 < z < b$ is easily derived,

$$\nabla^2\mathbf{u}_n = \nabla p_n + \mathcal{R}e((\mathbf{u}_0\cdot\nabla)\mathbf{u}_n + (\mathbf{u}_n\cdot\nabla)\mathbf{u}_0) + \mathcal{R}e\mathbf{F}_n, \quad \nabla\cdot\mathbf{u}_n = 0,\ n = 1,2,\ldots, \tag{2.11}$$

where

$$\mathbf{F}_n = \sum_{k=1}^{n-1}(\mathbf{u}_k\cdot\nabla)\mathbf{u}_{n-k}. \tag{2.12}$$

In order to deduce the boundary conditions for $\mathbf{u}_n$, the following formula is valid for a function $g(x, y, z)$ which is $(N + 1)$ differentiable with respect to z:

$$g(x,y,b\varepsilon B(x,y)) = \sum_{k=1}^{N}\frac{(b\varepsilon B(x,y))^k}{k!}\frac{\partial^k g}{\partial z^k}(x,y,0) + O(\varepsilon^{N+1}). \tag{2.13}$$

This formula is true for $N = \infty$ for a vanishing correction term if g is analytic with respect to z. However, this analyticity condition might be unnecessary. Therefore, we use in the following the formula with $N = \infty$ without any correction term as a shortcut notation,

$$g(x,y,b\varepsilon B(x,y)) = \sum_{k=1}^{\infty} \frac{(b\varepsilon B(x,y))^k}{k!} \frac{\partial^k g}{\partial z^k}(x,y,0). \tag{2.14}$$

Application of (2.14) and of a similar formula with $B(x, y)$ to (2.7) and use of (2.8) yield (for details, see [1] and [16])

$$\mathbf{u}_n(x,y,b) = \mathbf{0}, \quad \mathbf{u}_n(x,y,0) = \mathbf{H}_n(x,y), \tag{2.15}$$

where

$$\mathbf{H}_n(x,y) = -\sum_{k=1}^{n} \frac{(bB(x,y))^k}{k!} \frac{\partial^k \mathbf{u}_{n-k}}{\partial z^k}(x,y,0). \tag{2.16}$$

In each step, linear non-homogeneous equations with respect to $\mathbf{u}_n$ and p_n with the boundary conditions (2.15) have to be solved. The functions $\mathbf{u}_0$ and p_0 are given by (2.10). $\mathbf{u}_k$ and p_k ($k = 1,\ 2,\ldots,n-1$) are assumed to have been determined in the previous steps.

3 Reduction to ordinary differential equations

The method of separated variables can reduce Eqs. (2.11) and (2.15) to ordinary differential equations. All the functions are expanded as double Fourier series. It is convenient to use the Fourier series for real functions in complex form,

$$\begin{aligned}
u_n(x,y,z) &= \sum_{\xi,\eta=-\infty}^{\infty} \alpha_{\xi\eta}^{(n)}(z) e^{i(\xi x+\eta y)},\\
v_n(x,y,z) &= \sum_{\xi,\eta=-\infty}^{\infty} \beta_{\xi\eta}^{(n)}(z) e^{i(\xi x+\eta y)},\\
w_n(x,y,z) &= \sum_{\xi,\eta=-\infty}^{\infty} \gamma_{\xi\eta}^{(n)}(z) e^{i(\xi x+\eta y)},\\
p_n(x,y,z) &= \sum_{\xi,\eta=-\infty}^{\infty} \delta_{\xi\eta}^{(n)}(z) e^{i(\xi x+\eta y)},
\end{aligned} \tag{3.1}$$

$$\mathbf{F}_n(x,y,z) = \sum_{\xi,\eta=-\infty}^{\infty} \mathbf{F}_{\xi\eta}^{(n)}(z) e^{i(\xi x+\eta y)}, \quad \mathbf{H}_n(x,y) = \sum_{\xi,\eta=-\infty}^{\infty} \mathbf{H}_{\xi\eta}^{(n)} e^{i(\xi x+\eta y)}, \quad B(x,y) = \sum_{\xi,\eta=-\infty}^{\infty} B_{\xi\eta} e^{i(\xi x+\eta y)},$$

where $\mathbf{u}_n = (u_n,\ v_n,\ w_n)$. In each step n of the cascade, $\mathbf{F}_{\xi\eta}^{(n)}$ $\mathbf{H}_{\xi\eta}^{(n)}$ and $B_{\xi\eta}$ are known and the functions $\alpha_{\xi\eta}^{(n)}(z)$, $\beta_{\xi\eta}^{(n)}(z)$, $\gamma_{\xi\eta}^{(n)}(z)$, $\delta_{\xi\eta}^{(n)}(z)$ are unknown. For instance, Eqs. (3.1) can be detailed as

$$\begin{aligned}
u_n(x,y,z) = \alpha_{00}^{(n)}(z) &+ \sum_{\xi=1}^{\infty} \left(\alpha_{\xi 0}^{(n)}(z) e^{i\xi x} + \alpha_{-\xi 0}^{(n)}(z) e^{-i\xi x} \right) + \sum_{\eta=1}^{\infty} \left(\alpha_{0t}^{(n)}(z) e^{i\eta y} + \alpha_{0,-\eta}^{(n)}(z) e^{-i\eta y} \right)\\
&+ \sum_{\xi,\eta=1}^{\infty} \left(\alpha_{\xi\eta}^{(n)}(z) e^{i(\xi x+\eta y)} + \alpha_{\xi,-\eta}^{(n)}(z) e^{i(\xi x+\eta y)} + \alpha_{-\xi\eta}^{(n)}(z) e^{i(\xi x+\eta y)} + \alpha_{-\xi,-\eta}^{(n)}(z) e^{-i(\xi x+\eta y)} \right).
\end{aligned} \tag{3.2}$$

The function $\alpha_{00}^{(n)}(z)$ must be real. Consider the first sum in Eq. (3.2),

$$\sum_{\xi=1}^{\infty}\left(\alpha_{\xi 0}^{(n)}(z)e^{i\xi x}+\alpha_{-\xi 0}^{(n)}(z)e^{-i\xi x}\right)=\sum_{\xi=1}^{\infty}(a_{\xi}(z)\cos\xi x+b_{\xi}(z)\sin\xi x), \tag{3.3}$$

where $a_{\xi}(z)=\alpha_{\xi 0}^{(n)}(z)+\alpha_{-\xi 0}^{(n)}(z), b_{\xi}(z)=i(\alpha_{\xi 0}^{(n)}(z)-\alpha_{-\xi 0}^{(n)}(z))$. Since Eq. (3.3) is a usual Fourier series which must be real, one has

$$\alpha_{\xi 0}^{(n)}(z)=\frac{1}{2}(a_{\xi}(z)-ib_{\xi}(z)),\quad \alpha_{-\xi 0}^{(n)}(z)=\frac{1}{2}(a_{\xi}(z)+ib_{\xi}(z)). \tag{3.4}$$

The same arguments can be applied to the two other sums in (3.2). Therefore, it is possible to apply the complex ordinary series in (3.2) assuming that the conditions (3.4) are fulfilled. The condition that the velocity is real can be written as

$$\alpha_{-\xi,-\eta}(z)=\overline{\alpha_{\xi,\eta}(z)}, \tag{3.5}$$

where the overbar denotes complex conjugation. Similar conditions hold for the coefficients of the complex series (3.1).

Substitution of (3.1) into (2.11) and (2.15) and selection of the coefficients of the same modes $e^{i(\xi x+\eta y)}$ yield the four ordinary differential equations

$$\alpha''_{\xi\eta}(z)-\varkappa^2\alpha_{\xi\eta}(z)=i\xi\delta_{\xi\eta}(z)+\frac{\mathcal{R}e}{b}\left(iz\xi\alpha_{\xi\eta}(z)+\gamma_{\xi\eta}(z)\right)+\mathcal{R}eF_{\xi\eta}^{(1)}(z), \tag{3.6.1}$$

$$\beta''_{\xi\eta}(z)-\varkappa^2\beta_{\xi\eta}(z)=i\eta\delta_{\xi\eta}(z)+\frac{\mathcal{R}e}{b}iz\xi\beta_{\xi\eta}(z)+\mathcal{R}eF_{\xi\eta}^{(2)}(z), \tag{3.6.2}$$

$$\gamma''_{\xi\eta}(z)-\varkappa^2\gamma_{\xi\eta}(z)=\delta'_{\xi\eta}(z)+\frac{\mathcal{R}e}{b}iz\xi\gamma_{\xi\eta}(z)+\mathcal{R}eF_{\xi\eta}^{(3)}(z), \tag{3.6.3}$$

$$i\xi\alpha_{\xi\eta}(z)+i\eta\beta_{\xi\eta}(z)+\gamma'_{\xi\eta}(z)=0, \tag{3.6.4}$$

where $\varkappa=\sqrt{\xi^2+\eta^2}$, $\mathbf{F}_{\xi\eta}(z)=(F_{\xi\eta}^{(1)}(z),F_{\xi\eta}^{(2)}(z),F_{\xi\eta}^{(3)}(z))$ is a coordinate form of the vector-function (2.12). The superscript (n) is omitted for brevity. The boundary conditions follow from (2.15),

$$\alpha_{\xi\eta}(b)=0,\quad \alpha_{\xi\eta}(0)=H_{\xi\eta}^{(1)}, \tag{3.7}$$

$$\beta_{\xi\eta}(b)=0,\quad \beta_{\xi\eta}(0)=H_{\xi\eta}^{(2)},\quad \gamma_{\xi\eta}(b)=0,\quad \gamma_{\xi\eta}(0)=H_{\xi\eta}^{(3)}, \tag{3.8}$$

where, for instance, $\mathbf{H}_{\xi\eta}=(H_{\xi\eta}^{(1)},H_{\xi\eta}^{(2)},H_{\xi\eta}^{(3)})$ (see Eqs. (2.15)–(2.16)).

Equation (3.6.1) is multiplied by $i\xi$, Eq. (3.6.2) by $i\eta$ and the results are added. Then, Eq. (3.6.4) implies

$$-\gamma'''_{\xi\eta}(z)+\varkappa^2\gamma_{\xi\eta}(z)=-\varkappa^2\delta_{\xi\eta}(z)-\frac{\mathcal{R}e}{b}iz\xi\gamma'_{\xi\eta}(z)+\mathcal{R}e[isF_{\xi\eta}^{(1)}(z)+i\eta F_{\xi\eta}^{(2)}(z)]. \tag{3.9}$$

Differentiate[1] (3.9) and add Eq. (3.6) multiplied by $\varkappa^2$. As a result, a special case of the celebrated Orr–Sommerfeld equation is obtained [22], [23],

$$\gamma^{(IV)}-2\varkappa^2\gamma''+\varkappa^4\gamma=i\frac{\mathcal{R}e}{b}z\xi(\gamma''-\varkappa^2\gamma)+\mathcal{R}ef, \tag{3.10}$$

where

[1] We apply the operator of differentiation on the real variable z to complex functions.

$$f(z) = \mathcal{R}e(i\xi F^{(1)\prime}(z) + i\eta F^{(2)\prime}(z) + \varkappa^2 F^{(3)}(z)). \tag{3.11}$$

The subscripts $\xi\eta$ are omitted for brevity until the end of the present section. It follows from (3.7)–(3.8) and Eq. (3.6.4) that $\gamma(z)$ satisfies the boundary conditions

$$\gamma(0) = H^{(3)}, \quad \gamma'(0) = -i\xi H^{(1)} - i\eta H^{(2)}, \tag{3.12}$$

$$\gamma(b) = 0, \quad \gamma'(b) = 0. \tag{3.13}$$

As in [6], Eqs. (3.10)–(3.13) are reduced to a non-local problem with the new unknown function $\omega(z)$ defined as

$$\omega''(z) - \varkappa^2\omega(z) = i\xi\frac{\mathcal{R}e}{b}z\omega(z) + \mathcal{R}ef, \tag{3.14}$$

$$\gamma''(z) - \varkappa^2\gamma(z) = \omega(z). \tag{3.15}$$

Obviously, $\gamma(z)$ can be written as

$$\gamma(z) = c_1(z)e^{\varkappa z} + c_2(z)e^{-\varkappa z}. \tag{3.16}$$

Calculate the derivative

$$\gamma'(z) = c_1'(z)e^{\varkappa z} + c_2'(z)e^{-\varkappa z} + \varkappa(c_1(z)e^{\varkappa z} - c_2(z)e^{-\varkappa z}) \tag{3.17}$$

and put

$$c_1'(z)e^{\varkappa z} + c_2'(z)e^{-\varkappa z} = 0. \tag{3.18}$$

Calculate the second derivative

$$\gamma''(z) = \varkappa^2(c_1(z)e^{\varkappa z} + c_2(z)e^{-\varkappa z}) + \varkappa\big(c_1'(z)e^{\varkappa z} - c_2'(z)e^{-\varkappa z}\big). \tag{3.19}$$

Equations (3.15), (3.16) and (3.19) yield a second equation in $c_1^{'}$ and $c_2^{'}$,

$$c_1'(z)e^{\varkappa z} - c_2'(z)e^{-\varkappa z} = \frac{1}{\varkappa}\omega(z). \tag{3.20}$$

Therefore, (3.18) and (3.20) imply

$$c_1'(z) = \frac{1}{2\varkappa}\omega(z)e^{-\varkappa z}, \quad c_2'(z) = -\frac{1}{2\varkappa}\omega(z)e^{\varkappa z}. \tag{3.21}$$

These two relations can be integrated

$$\begin{aligned} c_1(z) &= \frac{1}{2\varkappa}\int_0^z e^{-\varkappa t}\omega(t)dt + c_1(0), \\ c_2(z) &= -\frac{1}{2\varkappa}\int_0^z e^{\varkappa t}\omega(t)dt + c_2(0), \end{aligned} \tag{3.22}$$

where $c_1(0)$ and $c_2(0)$ are constants which are determined by $z = 0$ using (3.12),

$$\gamma(0) = c_1(0) + c_2(0) = H^{(3)}, \quad \gamma'(0) = \varkappa(c_1(0) - c_2(0)) = -i\xi H^{(1)} - i\eta H^{(2)}. \tag{3.23}$$

The solution to the system (3.23) has the form

$$c_1(0) = \frac{1}{2\varkappa}(H^{(3)} - i\xi H^{(1)} - \eta H^{(2)}), \quad c_2(0) = \frac{1}{2\varkappa}(H^{(3)} + i\xi H^{(1)} + i\eta H^{(2)}). \tag{3.24}$$

Substitution of Eqs. (3.24) and (3.22) into (3.16) implies

$$\gamma(z) = \frac{1}{\varkappa}\int_0^z \sinh(\varkappa(z-t))\omega(t)dt + \frac{1}{\varkappa}(H^{(3)}\cosh\varkappa z - i(\xi H^{(1)} + \eta H^{(2)})\sinh\varkappa z). \tag{3.25}$$

Substitution of (3.25) into (3.13) yields the non-local problem for Eq. (3.14),

$$\begin{aligned}
&\int_0^b \sinh(\varkappa(b-t))\omega(t)dt = -H^{(3)}\cosh\varkappa b + i(\xi H^{(1)} + \eta H^{(2)})\sinh\varkappa b,\\
&\int_0^b \cosh(\varkappa(b-t))\omega(t)dt = -H^{(3)}\sinh\varkappa b + i(\xi H^{(1)} + \eta H^{(2)})\cosh\varkappa b.
\end{aligned} \tag{3.26}$$

Similar non-local forms of the problem were used to study the homogeneous Orr–Sommerfeld equation (see for instance [6]).

4 Solution

4.1 Solution to the non-local problem

In the present section, the ordinary differential equation (3.14) is solved with the non-local condition (3.26). First, a general solution of the homogeneous differential equation is found,

$$\omega_0''(z) = \left(\varkappa^2 + iz\frac{\xi\mathcal{R}e}{b}\right)\omega_0(z). \tag{4.1}$$

The solution can be expressed with the classical Airy's functions Ai(X) and Bi(X) (see [18]) which satisfy the ordinary differential equation $\mathrm{Ai}''(X) = X\mathrm{Ai}(X)$

$$\omega_0(z) = C_1\mathrm{Ai}\big[Z_{\xi\eta}(z)\big] + C_2\mathrm{Bi}\big[Z_{\xi\eta}(z)\big], \tag{4.2}$$

where C_1 and C_2 are undetermined constants; $Z_{\xi\eta}(z)$ is defined as

$$Z_{\xi\eta}(z) = -\left(\frac{b}{\xi\mathcal{R}e}\right)^{2/3}\left(\varkappa^2 + iz\frac{\xi\mathcal{R}e}{b}\right). \tag{4.3}$$

The choice of the fundamental solutions Ai(X) and Bi(X) is not essential from a theoretical point of view, but it is important in computations, since different pairs of the fundamental solutions are numerically satisfactory in different domains [18]. In this paper, Ai(X) denotes the commonly used first Airy's function. In Sect. 5, the second Airy's function Bi(X) is used. However, in Sect. 8, Ai($e^{2\pi/3}X$) is taken as the second fundamental solution Bi(X). Thus, all forthcoming formulas are valid with different pairs [Ai(X), Bi(X)]. Only one pair must be fixed for each step of the cascade.

The general solution of the non-homogeneous equation (3.14) is

$$\omega(z) = \omega_0(z) + \omega^*(z), \tag{4.4}$$

where ω*(z) denotes a particular solution of the non-homogeneous Eq. (3.14),

$$\omega^*(z) = \frac{i\pi\mathcal{R}e^{2/3}b^{1/3}}{\xi^{1/3}}\int_0^z \big(\mathrm{Bi}\big[Z_{\xi\eta}(z)\big]\mathrm{Ai}\big[Z_{\xi\eta}(t)\big] - \mathrm{Ai}\big[Z_{\xi\eta}(z)\big]\mathrm{Bi}\big[Z_{\xi\eta}(t)\big]\big)f(t)dt. \tag{4.5}$$

C_1 and C_2 are given by the conditions (3.26). First, introduce the integrals

$$
\begin{aligned}
J_{11}^{(\xi\eta)} &= \int_0^b \sinh(\varkappa(b-\zeta))\mathbf{Ai}\big[Z_{\xi\eta}(\zeta)\big]d\zeta,\\
J_{12}^{(\xi\eta)} &= \int_0^b \sinh(\varkappa(b-\zeta))\mathbf{Bi}\big[Z_{\xi\eta}(\zeta)\big]\mathrm{d}\zeta,\\
J_{21}^{(\xi\eta)} &= \int_0^b \cosh(\varkappa(b-\zeta))\mathbf{Ai}\big[Z_{\xi\eta}(\zeta)\big]\mathrm{d}\zeta,\\
J_{22}^{(\xi\eta)} &= \int_0^b \cosh(\varkappa(b-\zeta))\mathbf{Bi}\big[Z_{\xi\eta}(\zeta)\big]\mathrm{d}\zeta.
\end{aligned}
\tag{4.6}
$$

Substitution of (4.4) into (3.26) yields linear equations with respect to C_1 and C_2

$$
J_{11}^{(\xi\eta)}C_1 + J_{12}^{(\xi\eta)}C_2 = D_1, \quad J_{21}^{(\xi\eta)}C_1 + J_{22}^{(\xi\eta)}C_2 = D_2, \tag{4.7}
$$

where

$$
\begin{aligned}
D_1 &= -\int_0^b \sinh(\varkappa(b-t))\omega^*(t)dt - H^{(3)}\cosh\varkappa b + i(\xi H^{(1)} + \eta H^{(2)})\sinh\varkappa b,\\
D_2 &= -\int_0^b \cosh(\varkappa(b-t))\omega^*(t)dt - \sinh\varkappa b + i(\xi H^{(1)} + \eta H^{(2)})\cosh\varkappa b.
\end{aligned}
\tag{4.8}
$$

The solution of Eqs. (4.7) is

$$
C_1 = \frac{1}{\Delta^{(\xi\eta)}}\Big(D_2 J_{12}^{(\xi\eta)} - D_1 J_{22}^{(\xi\eta)}\Big), \quad C_2 = \frac{1}{\Delta^{(\xi\eta)}}\Big(D_1 J_{21}^{(\xi\eta)} - D_2 J_{11}^{(\xi\eta)}\Big), \tag{4.9}
$$

where

$$
\Delta^{(\xi\eta)} = J_{11}^{(\xi\eta)}J_{22}^{(\xi\eta)} - J_{12}^{(\xi\eta)}J_{21}^{(\xi\eta)}. \tag{4.10}
$$

The determinant $\Delta^{(\xi\eta)}$ cannot be 0. If $\Delta^{(\xi\eta)} = 0$, a non-zero solution of the Orr–Sommerfeld equation with zero boundary conditions would be obtained in a stationary case which is impossible according to [6].

Therefore, the non-local problem ((3.14), (3.26)) has been solved. The unique solution $\omega(z)$ has the form (4.2)–(4.4), and C_1 and C_2 are calculated by (4.9). The function $\gamma(z) = \gamma_{\xi\eta}^{(n)}(z)$ corresponding to the mode $e^{i(\xi x+\eta y)}$ can be expressed by (3.25).

To determine $\alpha_{\xi\eta}(z)$ and $\beta_{\xi\eta}(z)$ from (3.6) with known $\gamma_{\xi\eta}(z)$, the Eq. (3.6.1) multiplied by η is substracted from Eq. (3.6.2) multiplied by ξ. Then, $\delta(z)$ is eliminated. Further, we introduce

$$
\varpi_{\xi\eta}(z) := \eta\alpha_{\xi\eta}(z) - \xi\beta_{\xi\eta}(z). \tag{4.11}
$$

$\varpi_{\xi\eta}(z)$ verifies the following ordinary differential equation:

$$
\varpi''_{\xi\eta}(z) - \varkappa^2\varpi_{\xi\eta}(z) = \frac{\mathcal{R}e}{b}i\xi z\varpi_{\xi\eta}(z) + \frac{\mathcal{R}e}{b}\eta\gamma_{\xi\eta}(z) + \mathcal{R}e\Big(\eta F_{\xi\eta}^{(1)}(z) - \xi F_{\xi\eta}^{(2)}(z)\Big), \tag{4.12}
$$

with prescribed boundary values $\varpi_{\xi\eta}(0)$ and $\varpi_{\xi\eta}(b)$ derived from (3.7)–(3.8). Equation (4.12) has the same form as (3.14). The boundary value problem has a unique solution which can be written in a

closed form. Then, $\alpha_{\xi\eta}(z)$ and $\beta_{\xi\eta}(z)$ are easily found from (4.11) and Eq. (3.6.4). This will be done in Sect. 6 to the first order approximation in ε and in Sect. 8 with the precision $O(\varepsilon^4)$.

In the 2D case, the solution to the system (2.15) is simplified since $\beta_\xi(z) \equiv 0$ $(\eta = 0)$,

$$\varpi_\xi(z) = \alpha_{\xi\eta}(z) = \frac{i}{\xi}\gamma'_{\xi\eta}(z). \tag{4.13}$$

In Sect. 8, numerical results are presented in the 2D case. This section is ended with the presentation of the algorithm in details to compute $\alpha_\xi^{(n)}(z)$, $\gamma_\xi^{(n)}(z)$ through $\alpha_\xi^{(k)}(z), \gamma_\xi^{(k)}(z)(k = 0, 1, \ldots, n-1)$ in the 2D case. We have

$$\begin{aligned}
\alpha_\xi^{(n)}(z) &= -B_\xi\left(\cosh\xi z + \int_0^z \cosh\xi(\varsigma - z)(C_1\mathbf{Ai}[Z_\xi(\varsigma)] + C_2\mathbf{Bi}[Z_\xi(\varsigma)])d\varsigma\right) \\
&\quad + \int_0^z \cosh\xi(\varsigma - z)\mathbf{\Omega}(\varsigma)d\varsigma, \\
\gamma_\xi^{(n)}(z) &= iB_\xi\left(\sinh\xi z + \int_0^z \sinh\xi(\varsigma - z)(C_1\mathbf{Ai}[Z_\xi(\varsigma)] + C_2\mathbf{Bi}[Z_\xi(\varsigma)])d\varsigma\right) \\
&\quad + \int_0^z \sinh\xi(\varsigma - z)\mathbf{\Omega}(\varsigma)d\varsigma,
\end{aligned} \tag{4.14}$$

where

$$Z_\xi(z) = -\left(\frac{b}{\mathcal{R}e}\right)^{2/3}\xi^{1/3}\left(\xi + iz\frac{\mathcal{R}e}{b}\right). \tag{4.15}$$

The function $\mathbf{\Omega}(\zeta)$ is determined by

$$\mathbf{\Omega}(\zeta) = \frac{i\pi\mathcal{R}e^{2/3}b^{1/3}}{\xi^{1/3}}\int_0^\zeta (\mathbf{Ai}[Z_\xi(\zeta)]\mathbf{Bi}[Z_\xi(\zeta)] + \mathbf{Bi}[Z_\xi(\zeta)]\mathbf{Ai}[Z_\xi(\zeta)])f(\zeta)d\zeta, \tag{4.16}$$

where $f(z)$ is calculated by (3.11) with

$$\begin{aligned}
F^{(1)}(z) &= \sum_{k=1}^{n-1}\sum_{p=-\infty}^{\infty}\left(ip\alpha_{\xi-p}^{(k)}(z)\alpha_p^{(n-k)}(z) + \gamma_{\xi-p}^{(k)}(z)(\alpha_p^{(n-k)}(z))'\right), \quad F^{(2)}(z) = 0, \\
F^{(3)}(z) &= \sum_{k=1}^{n-1}\sum_{p=-\infty}^{\infty}\left(ip\alpha_{\xi-p}^{(k)}(z)\gamma_p^{(n-k)}(z) + \gamma_{\xi-p}^{(k)}(z)(\gamma_p^{(n-k)}(z))'\right).
\end{aligned} \tag{4.17}$$

The constants C_1 and C_2 are known from (4.9).

4.2 Convergence of the algorithm

The problem (2.6), (2.7) is now solved and the convergence of the series (2.8) has to be examined. Since this question is technical in character, it is fully addressed in Appendix A. It is proved that for a given wavy wall and a given Reynolds number, the supremum ε_c of ε can be expressed as

$$\varepsilon_c = \left[b \sup_{\xi,\eta} a_{\xi,\eta} \max\left(\sqrt{\xi^2+\eta^2}, \sqrt{\mathcal{R}e\sqrt{\xi^2+\eta^2}} \right) \right]^{-1}, \tag{4.18}$$

where $a_{\xi,\eta}$ is the maximum modulus from four coefficients of $e^{\pm i\xi \pm i\eta}$ in the double Fourier series of $2B(x, y)$. The proof of (4.18) is based on the estimations of the terms from the ordinary differential equations (3.6).

5 The first-order approximation in ε for a two-dimensional channel

5.1 General analytical formulas

As a first application of the previous section, the first-order approximation in ε for a two-dimensional channel with an arbitrary function $B(x, y) = B(x)$ is derived. The velocity can be written as

$$\mathbf{u}(x,z) = \left(\frac{z}{b}, 0\right) + \varepsilon(u_1(x,z), w_1(x,z)) + O(\varepsilon^2), \tag{5.1}$$

where $u_1(x, z)$ and $w_1(x, z)$ satisfy

$$\begin{aligned} \nabla^2 u_1 &= \frac{\partial p_1}{\partial x} + \frac{\mathcal{R}e}{b}\left(z\frac{\partial u_1}{\partial x} + w_1 \right), \\ \nabla^2 w_1 &= \frac{\partial p_1}{\partial z} + \frac{\mathcal{R}e}{b} z \frac{\partial w_1}{\partial x}, \\ \frac{\partial u_1}{\partial x} &+ \frac{\partial w_1}{\partial z} = 0, \end{aligned} \tag{5.2}$$

with the boundary conditions

$$u_1(x,b) = 0, \quad w_1(x,b) = 0, \quad u_1(x,0) = B(x), \quad w_1(x,0) = 0. \tag{5.3}$$

Therefore, the linear homogeneous problem (5.2)–(5.3) should be solved for the straight channel $0 < z < b$ (compare with the non-homogeneous equations (3.6)). Formulas (4.14) yield

$$\begin{aligned} \alpha_\xi^{(1)}(z) = -B_\xi \Bigg[&\cosh \xi z + \frac{(B^-(b) - B^+(b))A^-(z) + (A^+(b) - A^-(b))B^-(z)}{2\Delta} e^{\xi z} \\ &+ \frac{(B^-(b) - B^+(b))A^+(z) + (A^+(b) - A^-(b))B^+(z)}{2\Delta} e^{-\xi z} \Bigg], \\ \gamma_\xi^{(1)}(z) = iB_\xi \Bigg[&\sinh \xi z - \frac{(B^-(b) - B^+(b))A^-(z) + (A^+(b) - A^-(b))B^-(z)}{2\Delta} e^{\xi z} \\ &+ \frac{(B^-(b) - B^+(b))A^+(z) + (A^+(b) - A^-(b))B^+(z)}{2\Delta} e^{-\xi z} \Bigg], \end{aligned} \tag{5.4}$$

where B_ξ ($\xi = \pm 1, \pm 2 \ldots$) are coefficients of the complex Fourier series of $B(x) = B(x, y)$, the functions $A^\pm(z)$ and $B^\pm(z)$ are defined via integrals

$$A^\pm(z) = \int_0^z \mathrm{Ai}[Z_\xi(\zeta)] e^{\pm\xi z} d\zeta, \quad B^\pm(z) = \int_0^z \mathrm{Bi}[Z_\xi(\zeta)] e^{\pm\xi z} d\zeta, \tag{5.5}$$

and the constant Δ is introduced as follows:

$$\Delta = A^+(b)B^-(b) - A^-(b)B^+(b). \tag{5.6}$$

The functions u_1 and w_1 have the form

$$u_1(x,z) = \sum_{\xi=-\infty}^{\infty} \alpha_\xi^{(1)}(z) e^{i\xi x}, \quad w_1(x,z) = \sum_{\xi=-\infty}^{\infty} \beta_\xi^{(1)}(z) e^{i\xi x}. \tag{5.7}$$

The exact formulas (5.4)–(5.7) and the approximate one (5.1) can be used to study the structure of the flow in the channel up to $O(\varepsilon^2)$. First, the critical value $\varepsilon_e = \varepsilon_e(\mathcal{R}e)$ of the start of an eddy in the channel is determined, as well as the location of separation points lying on the walls and the curve limiting the recirculation region.

Introduce the function

$$f(x,\varepsilon) = \frac{1}{b} + \varepsilon \frac{\partial u_1}{\partial z}(x,0) \tag{5.8}$$

which is the bottom wall shear stress up to $O(\varepsilon^2)$. According to [22], a separation point is a point $(x,\, b\varepsilon\, B(x))$ for which

$$f(x,\varepsilon) = 0. \tag{5.9}$$

Use Eqs. (5.4) to calculate

$$\frac{\partial u_1}{\partial z}(x,0) = \sum_{\xi=-\infty}^{\infty} (\alpha_\xi^{(1)}(z))'_{z=0} e^{i\xi x} = 2\mathrm{Re} \sum_{\xi=1}^{\infty} (\alpha_\xi^{(1)}(z))'_{z=0} e^{i\xi x}, \tag{5.10}$$

where Re stands for the real part. Therefore, $f(x,\varepsilon)$ can be expressed as

$$f(x,\varepsilon) = \frac{1}{b} + \varepsilon 2\mathrm{Re} \sum_{\xi=1}^{\infty} (\alpha_\xi^{(1)}(\mathrm{z}))'_{\mathrm{z}=0} \mathrm{e}^{\mathrm{i}\xi\mathrm{x}}. \tag{5.11}$$

It is assumed that the series (5.11) converges. The case of divergent series will be also considered in the next Subsection. Equation (5.1) shows that Eq. (5.9) with respect to x has not a solution for all ε. For instance, $f(x,0) = \frac{1}{b} > 0$. Hence, for small positive ε, the function $f(x,\varepsilon)$ is positive whatever x. A minimal value ε_e is expected to exist for which

$$f(x,\varepsilon_e) = 0. \tag{5.12}$$

Let $\varepsilon = \varepsilon_e$ be the critical point of the start of an eddy in the channel. Then, (5.4) implies

$$\varepsilon_e = -\left[4b\mathrm{Re} \sum_{\xi=1}^{\infty} \mathrm{e}^{i\xi \mathrm{x_e}} \frac{B_\xi}{\Delta^{(\xi)}} \int_0^{\mathrm{b}} (\mathrm{Ai}[Z_\xi(0)]\mathrm{Bi}[Z_\xi(\zeta)] - \mathrm{Bi}[Z_\xi(0)]\mathrm{Ai}[Z_\xi(\zeta)]) \sinh \xi\zeta \mathrm{d}\zeta \right]^{-1}, \tag{5.13}$$

where x_e is the root of Eq. (5.12).

5.2 Dependence of ε_e on the wall smoothness

In the present subsection, the dependence of ε_e on the wall smoothness is estimated via the convergence rate of the Fourier coefficients of $B(x)$. Hereafter, a compact and physically intuitive notation is adopted:

$$\begin{aligned} &X \prec Y, \quad \text{whenever} \quad X \le cY, \\ &X \sim Y, \quad \text{whenever} \quad c^{-1}Y \le X \le cY, \end{aligned} \tag{5.14}$$

for a suitable constant $c \ge 1$. The relation $\prec$ is used only for non negative values; $\sim$ is valid for all real values.

Introduce the function $\mathcal{F}(x)$ via its Fourier series

$$\mathcal{F}(x) = \sum_{\xi=-\infty}^{+\infty} B_\xi \Lambda_\xi e^{i\xi x}, \tag{5.15}$$

where

$$\Lambda_\xi = \frac{2}{\Delta^{(\xi)}} \int_0^b (\mathrm{Ai}[Z_\xi(0)]\mathrm{Bi}[Z_\xi(\zeta)] - \mathrm{Bi}[Z_\xi(0)]\mathrm{Ai}[Z_\xi(\zeta)]) \sinh \xi\zeta d\zeta, \tag{5.16}$$

$\Delta^{(\xi)}$ has the form (4.10). Then, according to (5.13), the critical ε_e at the onset of eddies can be written as

$$\varepsilon_e = -[b\mathcal{F}(x_e)]^{-1}. \tag{5.17}$$

For small $\mathcal{R}e$, Λ_ξ can be estimated as follows. Application of formula $\mathrm{A}i(x_0 + \Delta x) = \mathrm{A}i(x_0) + \mathrm{A}i'(x_0)\Delta x + O(\Delta x^2)$ with $x_0 = Z_\xi(0) = -(b\xi^2\mathcal{R}e^{-1})^{2/3}$ and $\Delta x = -iz\ (b^{-1}\xi\mathcal{R}e)^{1/3}$ yields

$$\mathrm{Ai}[Z_\xi(z)] = \mathrm{Ai}[Z_\xi(0)] + \mathrm{Ai}'[Z_\xi(0)](-iz(\mathrm{b}^{-1}\xi\mathcal{R}\mathrm{e})^{1/3}) + \mathrm{O}((\mathcal{R}\mathrm{e})^{2/3}). \tag{5.18}$$

This implies

$$\mathrm{Ai}[Z_\xi(0)]\mathrm{Bi}[Z_\xi(z)] - \mathrm{Bi}[Z_\xi(0)]\mathrm{Ai}[Z_\xi(z)] = \frac{\mathrm{i}z}{\pi}(b^{-1}\xi\mathcal{R}\mathrm{e})^{1/3} + \mathrm{O}((\mathcal{R}\mathrm{e})^{2/3}). \tag{5.19}$$

Here, the identity $\mathrm{Ai}(x)\mathrm{Bi}'(x) - \mathrm{Bi}(x)\mathrm{Ai}'(x) = \frac{1}{\pi}$ is used for the Wronskian of Airy's functions [18].

Consider the first integral (4.6) for a two dimensional channel

$$J_{11}^{(\xi)} = \int_0^b \sinh(\xi(b-\zeta))\mathrm{Ai}[Z_\xi(\zeta)]\mathrm{d}\zeta. \tag{5.20}$$

Application of (5.18) to (5.20) yields

$$J_{11}^{(\xi)} = \mathrm{Ai}[Z_\xi(0)]\frac{\cosh b\xi - 1}{\xi} - \mathrm{Ai}'[Z_\xi(0)]\frac{\sinh b\xi - b\xi}{\xi^2} i(b^{-1}\xi\mathcal{R}\mathrm{e})^{1/3} + \mathrm{O}((\mathcal{R}\mathrm{e})^{2/3}). \tag{5.21}$$

The other integrals in (4.6) are estimated in the same way. Then, $\Delta^{(\xi)}$ (see (4.10)) becomes

$$\Delta^{(\xi)} = \frac{i}{\pi\xi^3}(b^{-1}\xi\mathcal{R}e)^{1/3}(2\cosh b\xi - b\xi\sinh b\xi - 2) + O((\mathcal{R}e)^{2/3}). \tag{5.22}$$

Finally, Λ_ξ is obtained by substitution of (5.19) and (5.22) into (5.16),

$$\Lambda_\xi = \xi\ \frac{b\xi\cosh b\xi - \sinh b\xi}{2\cosh b\xi - b\xi\sinh b\xi - 2} + O((\mathcal{R}e)^{2/3}). \tag{5.23}$$

One can see that Λ_ξ is of order ξ when ξ tends to infinity.

5.3 Application to walls with non smooth points

Consider a continuous periodic function $B(x)$ with non-smooth points when $B'(x)$ is continuous except at a finite set of points with finite increments. In this case ([4], p. 270),

$$|B_\xi| \prec \frac{1}{\xi^2} \quad \text{as} \quad \xi \to +\infty. \tag{5.24}$$

Hence, $|B_\xi \Lambda_\xi| \prec \frac{1}{\xi}$ and the series (5.15) can converge. In order to investigate this situation, it is sufficient to consider a wall with one corner point, since the behavior of the Fourier series at x_0 corresponding to a function $f(x)$ depends only on the values of $f(x)$ in the neighborhood of x_0 ([4], p. 272).

Let $B(x)$ be a continuous 2π-periodic function, continuously differentiable in $[-\pi, \pi]$ except at a point x_0, where the limit values $B'(x_0 + 0)$ and $B'(x_0 - 0)$ are finite, but different. For simplicity, it is assumed that $B''(x)$ is continuous in $[-\pi, \pi]$, except at x_0 where $B''(x_0) = \infty$. Without any loss of generality, one can choose $x_0 = 0$ since $B(x)$ is periodic.

In order to estimate the Fourier coefficient

$$B_\xi = \frac{1}{2\pi} \int_{-\pi}^{\pi} B(x) e^{-i\xi x}\, dx \tag{5.25}$$

integration by parts is applied,

$$B_\xi = -\frac{i}{2\pi\xi} \int_{-\pi}^{\pi} B'(x) e^{-i\xi x}\, dx. \tag{5.26}$$

Introduce a small positive parameter δ. The function $B(x)$ can be changed on the segment $-\delta < x < \delta$ by a new function $\hat{B}(x)$ in such a way that $\hat{B}(x)$ is twice differentiable in $(-\pi, \pi)$. The precise form of $\hat{B}(x)$ is not important. Divide the segment of integration into three segments $(-\pi, \delta)$, $(-\delta, \delta)$, (δ, π). Then, (5.26) implies

$$B_\xi = \hat{B}_\xi + D_\xi, \tag{5.27}$$

where the Fourier coefficient of $\hat{B}(x)$ is defined as

$$\hat{B}_\xi = -\frac{i}{2\pi\xi} \int_{-\pi}^{\pi} \hat{B}'(x) e^{-i\xi x}\, dx. \tag{5.28}$$

Moreover,

$$D_\xi = -\frac{i}{2\pi\xi} \int_{-\delta}^{\delta} (B'(x) - \hat{B}'(x)) e^{-i\xi x}\, dx. \tag{5.29}$$

Estimate now the real part of D_ξ written in the form

$$Re D_\xi = -\frac{1}{2\pi\xi} \int_0^{\delta} [B'(x) - B'(-x) - \hat{B}'(x) + \hat{B}'(-x)] \sin \xi x\, dx. \tag{5.30}$$

Application of the second theorem of the mean value to the integral (5.30) yields

$$Re D_\xi = -\frac{c_0}{2\pi\xi} \int_0^{x_\delta} \sin \xi x\, dx = -\frac{c_0}{\pi\xi^2} \sin^2 \frac{x_\delta \xi}{2}, \tag{5.31}$$

where $0 < x_\delta < \delta$, $c_0 = [B'(+0) - B'(-0)] \neq 0$ is the increment of $B'(x)$ when x passes through $x = 0$. Therefore, the coefficient of $\frac{1}{\xi^2}$ does not vanish. Let sign c_0 denote the sign of c_0. Then, (5.31) implies

$$ReD_\xi \sim -\frac{\text{sign } c_0}{\xi^2}. \tag{5.32}$$

Application of (5.27) to (5.32) yields

$$ReB_\xi \sim -\frac{\text{sign } c_0}{\xi^2}, \tag{5.33}$$

since $|\hat{B}_\xi| \prec \frac{1}{|\xi|^3}$ are Fourier coefficients of twice differentiable functions [4]. The estimation (5.33) provides the exact scale for B_ξ, because one can check that $\text{Im}D_\xi \prec \frac{1}{\xi^2}$.

The value of $\mathcal{F}(x)$ defined by (5.15) at the corner point $x = 0$ is exactly estimated for small $\mathcal{R}e$ as follows:

$$\mathcal{F}(0) \sim -2 \text{ sign } c_0 \sum_{\xi=1}^{+\infty} \frac{1}{\xi}. \tag{5.34}$$

One can show that $\mathcal{F}(0) = \infty$ with a sign which depends on the sign of c_0. This observation can be used as follows. Instead of $B(x) = 2Re \sum_{\xi=1}^{+\infty} B_\xi e^{i\xi x}$, consider a truncated sum $B_M(x) = 2\text{Re} \sum_{\xi=1}^{M} B_\xi e^{i\xi x}$. The function $B_M(x)$ defines a smooth wall of the channel. The critical value of ε can be calculated by (5.17),

$$\varepsilon_e^{(M)} = -[b\mathcal{F}_M(x_e)]^{-1}, \tag{5.35}$$

where the following function is properly determined on $[-\pi, \pi]$:

$$\mathcal{F}_M(x) = 2\text{Re} \sum_{\xi=1}^{\text{M}} \text{B}_\xi \Lambda_\xi \text{e}^{\text{i}\xi\text{x}}. \tag{5.36}$$

When M tends to infinity, $\mathcal{F}_M(x)$ becomes unbounded near $x = 0$ and $[\mathcal{F}_M(x)]^{-1}$ tends to zero. The sign of $\varepsilon_e^{(M)}$ from (5.35) must be verified, because only the case $\varepsilon_e^{(M)} \geq 0$ is allowed.

If $c_0 > 0, \mathcal{F}(0) = -\infty$ and (5.35) yields $\varepsilon_e = +0$. If $c_0 < 0$, $\mathcal{F}_M(0)$ tends to $+\infty, \mathcal{F}_M(x) > 0$ near $x = 0$. Then, the tangent component of the velocity on the bottom tends to $+\infty$ at $x = 0$; hence, it is positive near $x = 0$. Let θ^+ be the angle between the curve $B(x)$ and the axis OX at the point $x = 0$ from the right hand side, θ^- from the left hand side. Then, $c_0 = \tan \theta^+ - \tan \theta^-$ and the sign of c_0 admits the following simple geometrical interpretation. If the angle at $x = 0$ between the edges of the bottom wall is acute, eddies occur for infinitesimally small ε. The case of an obtuse angle can be treated as a liquid jet (see [13], p. 210 for details).

Thus, *eddies always arise for $\mathcal{R}e = 0$ in a non–smooth channel near a corner point with acute interior angle* (compare to [15]).

Consider a channel with a smooth wall, i.e., a function $B(x)$ continuously differentiable on $[-\pi, \pi]$ with the period 2π. In this case, the Fourier coefficients satisfy the asymptotics

$$|B_\xi| \sim \frac{1}{\xi^3} \quad \text{as} \quad \xi \to +\infty. \tag{5.37}$$

Then, the series (5.15) always converges for any fixed Reynolds number. This means that for smooth walls eddies do not arise suddenly near $\varepsilon = 0$ as for non–smooth walls. The value of ε_e is calculated by (5.13) which yields a finite number.

Finally, it is important to recall that the calculations of this section are performed in the range $\varepsilon < \varepsilon_c$ where $\varepsilon_c = (b \sup_\xi |2B_\xi \xi|)^{-1} \sim b^{-1}$ is given by (4.18).

6 The first-order approximation for 3D channels

The general algorithm presented in Sect. 4 is now used to derive the first-order approximation in ε for the 3D channels bounded by the walls $z = 0$ and $z = B(x, y)$, where $B(x, y)$ is an arbitrary function expanded as a Fourier series. The velocity can be written as

$$\mathbf{u}(x,y,z) = \left(\frac{z}{b}, 0, 0\right) + \varepsilon(u_1(x,y,z), v_1(x,y,z), w_1(x,y,z)) + O(\varepsilon^2), \tag{6.1}$$

where u_1, v_1, w_1 are Fourier expanded with unknown coefficients satisfying the equation

$$\alpha^{(n)}_{\xi\eta}(z) = \overline{\alpha^{(n)}_{-\xi,-\eta}(z)}. \tag{6.2}$$

Hereafter, the superscript $n = 1$ is omitted. Substitution of (3.1) into (2.11) and (2.15) with $n = 1$, and selection of the coefficients of the same modes $e^{i(\xi x+\eta y)}$ imply ordinary differential equations (see (3.6)) which are different in the following four cases ($\xi \neq 0$, η=0), (ξ =0, η=0), (ξ =0, $\eta \neq$ 0), ($\xi \neq 0$, $\eta \neq 0$) which are considered separately.

The case $\xi \neq 0$, η=0 corresponds to the 2D channel studied in Sect. 5 for which the final formulas of Sect. 5 can be used.

6.1 The case $\xi = \eta = 0$

This case is the simplest one. The coefficients of the constant terms verify

$$\begin{aligned}
&\alpha''_{00}(z) = R\gamma_{00}(z),\\
&\beta''_{00}(z) = 0,\\
&\gamma''_{00}(z) = \delta'_{00}(z),\\
&\gamma'_{00}(z) = 0,
\end{aligned} \tag{6.3}$$

where

$$R = \frac{\mathcal{R}e}{b}. \tag{6.4}$$

The functions α_{00}, β_{00}, γ_{00} vanish at the end points $z = 0$ and $z = b$, since $B(x, y)$ does not contain the (0, 0) term in its Fourier expansion (see (2.2)). It is easily seen that the latter boundary value problem has only the trivial solution $\delta_{00}(z) =$ constant.

6.2 The case $\xi = 0$, $\eta \neq 0$

This case $\xi = 0$, $\eta \neq 0$ corresponds to a Couette flow bounded by the walls $z = b$ and $z = b\varepsilon B(y)$ when the wall $z = b$ is moved along the x-direction. This case is not more difficult. The coefficients of $e^{i\eta y}$ ($\eta =$ ±1, ±2, ...) verify

$$\alpha''_{0\eta}(z) - \eta^2\alpha_{0\eta}(z) = R\gamma_{0\eta}(z), \tag{6.5.1}$$

$$\beta''_{0\eta}(z) - \eta^2\beta_{0\eta}(z) = i\eta\delta_{0\eta}(z), \tag{6.5.2}$$

$$\gamma''_{0\eta}(z) - \eta^2\gamma_{0\eta}(z) = \delta'_{0\eta}(z), \tag{6.5.3}$$

$$i\eta\beta_{0\eta}(z) + \gamma'_{0\eta}(z) = 0, \tag{6.5.4}$$

with the following boundary conditions:

$$\alpha_{0\eta}(0) = -B_{0\eta}, \quad \alpha_{0\eta}(b) = \beta_{0\eta}(0) = \beta_{0\eta}(b) = \gamma_{0\eta}(0) = \gamma_{0\eta}(b) = 0. \tag{6.6}$$

Elimination of $\delta_{0\eta}$ between Eqs. (6.5.2) and (6.5.3) implies

$$\Big(\beta'_{0\eta}(z) - i\eta\gamma_{0\eta}(z)\Big)'' - \eta^2\Big(\beta'_{0\eta}(z) - i\eta\gamma_{0\eta}(z)\Big) = 0. \tag{6.7}$$

Elimination of $\beta_{0\eta}$ between Eqs. (6.5.4) and (6.7) yields an ordinary differential equation of the fourth order with constant coefficients with respect to $\gamma_{0\eta}(z)$,

$$\Big(\gamma''_{0\eta}(z) - \eta^2\gamma_{0\eta}(z)\Big)'' - \eta^2\Big(\gamma''_{0\eta}(z) - \eta^2\gamma_{0\eta}(z)\Big) = 0. \tag{6.8}$$

It follows from Eqs. (6.5.4) and (6.6) that

$$\gamma_{0\eta}(0) = \gamma_{0\eta}(b) = \gamma'_{0\eta}(0) = \gamma'_{0\eta}(b) = 0. \tag{6.9}$$

It is easily seen that the boundary value problem (6.8)–(6.9) has only a trivial solution. Then, Eq. (6.5.4) implies that $\beta_{0\eta}(z) = 0$; hence, because of Eq. (6.5.3) $\delta_{0\eta}(z) = 0$.

Thus, the homogeneous equation is obtained,

$$\alpha''_{0\eta}(z) - \eta^2\alpha_{0\eta}(z) = 0, \tag{6.10}$$

with the boundary conditions

$$\alpha_{0\eta}(0) = -B_{0\eta}, \quad \alpha_{0\eta}(b) = 0. \tag{6.11}$$

The solution of this elementary problem (6.10), (6.11) is

$$\alpha_{0\eta}(z) = -B_{0\eta}\frac{\sinh\eta(b-z)}{\sinh\eta b}. \tag{6.12}$$

6.3 The case $\xi \neq 0$, $\eta \neq 0$

This case $\xi \neq 0$, $\eta \neq 0$ corresponds to the Couette flow in the most general channel bounded by three dimensional walls. The coefficients of $e^{i(\xi x+\eta y)}$ are selected to obtain (see (3.6))

$$\begin{aligned}
&\alpha''_{\xi\eta}(z) - \varkappa^2\alpha_{\xi\eta}(z) = i\xi\delta_{\xi\eta}(z) + R\big(iz\alpha_{\xi\eta}(z) + \gamma_{\xi\eta}(z)\big),\\
&\beta''_{\xi\eta}(z) - \varkappa^2\beta_{\xi\eta}(z) = i\eta\delta_{\xi\eta}(z) + Riz\beta_{\xi\eta}(z),\\
&\gamma''_{\xi\eta}(z) - \varkappa^2\gamma_{\xi\eta}(z) = \delta'_{0\eta}(z) + Riz\gamma_{\xi\eta}(z),\\
&i\xi\alpha_{\xi\eta}(z) + i\eta\beta_{\xi\eta}(z) + \gamma'_{\xi\eta}(z) = 0
\end{aligned} \tag{6.13}$$

with the boundary conditions

$$\alpha_{\xi\eta}(0) = -B_{\xi\eta}, \quad \alpha_{\xi\eta}(b) = \beta_{\xi\eta}(0) = \beta_{\xi\eta}(b) = \gamma_{\xi\eta}(0) = \gamma_{\xi\eta}(b) = 0. \tag{6.14}$$

The function $\gamma_{\xi\eta}(z)$ is given in Section 3 by formula (3.25) which becomes

$$\gamma_{\xi\eta}(z) = \frac{1}{\varkappa}\int_0^z \sinh\varkappa(z-\tau)\omega_{\xi\eta}(\tau)d\tau + \frac{i\xi}{\varkappa}B_{\xi\eta}\sinh\varkappa z, \tag{6.15}$$

where $\omega_{\xi\eta}(\{z\})$ has the form (4.2)–(4.4). In formula (4.2), the constants C_1 and C_2 are calculated by (49) where $J_{pq}^{(\xi\eta)}$ is introduced in (4.6) and

$$D_1 = -\int_0^b \sinh \varkappa(b-\tau)\omega^*(\tau)d\tau - i\xi B_{\xi\eta} \sinh \varkappa b,$$

$$D_2 = -\int_0^b \cosh \varkappa(b-\tau)\omega^*(\tau)d\tau - i\xi B_{\xi\eta} \cosh \varkappa b,$$

where $\omega^*(\tau)$ has the form (4.5). $\alpha_{\xi\eta}$ and $\beta_{\xi\eta}$ can be obtained by the ordinary differential equation derived from (4.12),

$$\varpi''_{\xi\eta}(z) - \varkappa^2 \varpi_{\xi\eta}(z) = i\xi R \varpi_{\xi\eta}(z) + R\eta\gamma_{\xi\eta}(z). \tag{6.16}$$

The boundary conditions are given by (3.7)–(3.8),

$$\varpi_{\xi\eta}(0) = -B_{\xi\eta}, \quad \varpi_{\xi\eta}(b) = 0. \tag{6.17}$$

Equation (6.16) is similar to (3.14). Its solution is found by the same method

$$\varpi_{\xi\eta}(z) = (C_3 + \Gamma_B(z))\mathrm{Ai}\big[Z_{\xi\eta}(z)\big) + (C_4 - \Gamma_A(z))\mathrm{Bi}\big(Z_{\xi\eta}(z)\big), \tag{6.18}$$

where

$$\Gamma_A(z) = -i\pi z \sqrt[3]{\frac{R^2}{\xi}} \int_0^z \mathrm{Ai}\big[Z_{\xi\eta}(\tau)\big)\gamma_{\xi\eta}(\tau)d\tau,$$

$$\Gamma_B(z) = -i\pi z \sqrt[3]{\frac{R^2}{\xi}} \int_0^z \mathrm{Bi}\big[Z_{\xi\eta}(\tau)\big)\gamma_{\xi\eta}(\tau)d\tau,$$

$$C_3 = \frac{1}{D_{\xi\eta}}\left[\left(\mathrm{Bi}\big[Z_{\xi\eta}(b)\big)\Gamma'_A(b) + \frac{\xi^2-\eta^2}{\xi^2+\eta^2}\mathrm{Ai}\big[Z_{\xi\eta}(b)\big)\Gamma'_A(b)\right)\mathrm{Bi}\big[Z_{\xi\eta}(0)\big) + \eta B_{\xi\eta}\mathrm{Bi}\big[Z_{\xi\eta}(b)\big)\right],$$

$$C_4 = -\frac{1}{D_{\xi\eta}}\left[\left(\mathrm{Bi}\big[Z_{\xi\eta}(b)\big)\Gamma'_A(b) + \frac{\xi^2-\eta^2}{\xi^2+\eta^2}\mathrm{Ai}\big[Z_{\xi\eta}(b)\big)\Gamma'_A(b)\right)\mathrm{Ai}\big[Z_{\xi\eta}(0)\big) + \eta B_{\xi\eta}\mathrm{Ai}\big[Z_{\xi\eta}(b)\big)\right],$$

and

$$D_{\xi\eta} = \mathrm{Ai}\big[Z_{\xi\eta}(\mathrm{b})\big)\mathrm{Bi}\big[Z_{\xi\eta}(0)\big) - \mathrm{Ai}\big[Z_{\xi\eta}(0)\big)\mathrm{Bi}\big[Z_{\xi\eta}(\mathrm{b})\big). \tag{6.19}$$

The functions $\alpha_{\xi\eta}(z)$ and $\beta_{\xi\eta}(z)$ are the solutions of the set of equations (see the last equality (2.15) and (4.11))

$$\begin{aligned} &\xi\alpha_{\xi\eta}(z) + \eta\beta_{\xi\eta}(z) = i\gamma'_{\xi\eta}(z), \\ &\eta\alpha_{\xi\eta}(z) - \eta\beta_{\xi\eta}(z) = \varpi_{\xi\eta}(z). \end{aligned} \tag{6.20}$$

Ultimately,

$$\alpha_{\xi\eta}(z) = \frac{1}{\varkappa^2}\Big(i\xi\gamma'_{\xi\eta}(z) + \eta\varpi_{\xi\eta}(z)\Big),$$

$$\beta_{\xi\eta}(z) = -\frac{1}{\varkappa^2}\Big(\xi\varpi_{\xi\eta}(z) - i\eta\gamma'_{\xi\eta}(z)\Big),$$

where $\gamma_{\xi\eta}{}'(z)$ is calculated by (6.15) as

$$\gamma'_{\xi\eta}(z) = \int_0^z \cosh \varkappa(z-\tau)\omega_{\xi\eta}(\tau)d\tau + i\xi B_{\xi\eta} \cosh \varkappa z. \tag{6.21}$$

$\omega_{\xi\eta}(z)$ has the form (4.2)–(4.4); $\varpi_{\xi\eta}(z)$ is given by (6.18). It is worth noticing that the above formulas for $\alpha_{\xi\eta}$, $\beta_{\xi\eta}$ and $\gamma_{\xi\eta}$ are exact, i.e., these functions have been found in closed form.

The velocity $\mathbf{u}(x, y, z)$ is calculated up to $O(\varepsilon^2)$ by (6.1), where for instance

$$u_1(x,y,z) = \sum_{\xi,\eta=-\infty}^{\infty} \alpha_{\xi\eta}(\tau)e^{i(\xi x+\eta y).} \tag{6.22}$$

Using (6.2), it is sufficient to calculate $\alpha_{\xi\eta}(z)$ only for non-negative ξ. Then, (6.22) becomes

$$u_1(x,y,z) = 2\mathrm{Re}\left(\sum_{\xi=1}^{\infty} \alpha_{\xi 0}(z)e^{i\xi x} + \sum_{\eta=1}^{\infty} \alpha_{0\eta}(z)e^{i\eta y} + \sum_{\xi=1}^{\infty}\sum_{\eta=-\infty}^{\infty} \alpha_{\xi\eta}(z)e^{i(\xi x+\eta y)}\right), \tag{6.23}$$

where the term $\eta = 0$ is omitted in the last sum. Here, we use the relation $\alpha_{00}(z) = 0$ (see Sect. 6.1). Similar formulas are valid for v_1 and w_1.

7 Separation in 3D channels

Following Subsect. 5.1 and using the results of Sect. 6 in the present section, the boundary layer separation flow in 3D channels (according to the terminology of [44], p. 201) is discussed up to $O(\varepsilon^2)$. First, consider 2D channels bounded by the walls

$$z = b, \quad z = b\varepsilon B_{2D}(x), \tag{7.1}$$

where a smooth function $B_{2D}(x)$ is represented by its Fourier series

$$B_{2D}(x) := \sum_{\xi=1}^{\infty} 2\mathrm{Re}\big(B_{\xi 0}e^{i\xi x}\big). \tag{7.2}$$

Let the Reynolds number be fixed and ε be a variable parameter. Let $S_{2D}(\varepsilon)$ be the projection of the flow recirculation regions onto the plane (x, y); of course, $S_{2D}(\varepsilon)$ is a strip parallel to the y-axis. According to Subsect. 5.1, the set $S_{2D}(\varepsilon)$ is empty for $\varepsilon < \varepsilon_e^{(2D)}$; it may contain several lines parallel to the y-axis[2] for $\varepsilon = \varepsilon_e^{(2D)}$. For $\varepsilon > \varepsilon_e^{(2D)}$, it consists of strips and lines parallel to the y-axis.

Consider now a perturbation of the 2D channel (7.1) which is a 3D channel bounded by the walls

$$z = b, \quad z = b\varepsilon B(x, y), \tag{7.3}$$

where

$$B(x, y) = B_{2D}(x) + G(x, y). \tag{7.4}$$

Here, the double Fourier series of $G(x, y)$ consists of the terms $B_{\xi\eta}\, e^{i(\xi x+\eta y)}$ with $\eta \neq 0$. Further, we say that the 2D channel (7.1) corresponds to the 3D channel (7.3).

Define the set $S(\varepsilon)$ on the plane (x, y) in the following way. Let $\mathrm{P}_{x_0y_0}$ be the plane tangent to the surface $z = b\varepsilon B(x, y)$ at the point (x_0, y_0). Let $\mathbf{n}$ be the unit normal vector to $\mathrm{P}_{x_0y_0}$, and $\mathbf{t}(x_0, y_0)$ a unit vector normal to $\mathbf{n}$ and such that its y-component vanishes. u_t is the component of the velocity $\mathbf{u}$ at $(x_0\ y_0,\ b\varepsilon B(x_0\ y_0))$ along $\mathbf{t}$. The boundary of $S(\varepsilon)$ is defined by

[2] In most cases, the set $S_{2D}(\varepsilon_e^{(2D)})$ for the critical value of ε contains only one line.

$$\frac{\partial u_t}{\partial n} = 0. \tag{7.5}$$

As in the 2D dimensional case, Eq. (7.5) up to $O(\varepsilon^2)$ can be written in the form

$$\frac{1}{b} + \varepsilon \frac{\partial u_1}{\partial z}(x, y, 0) = 0, \tag{7.6}$$

where $u_1(x, y, z)$ is the coefficient in ε of the x-component of the velocity in the 3D channel. Now we deduce a formula connecting $u_1(x, y, z)$ for the 3D channel and $u_{2D}(x, z)$, the coefficient in ε of the x component of the velocity of the corresponding 2D channel. The coefficient $\alpha_{\xi\eta}(z)$ from (6.23) is proportional to $B_{\xi\eta}$. For $B_{\xi 0}$, it follows directly from (5.4). For $B_{\xi\eta}$ ($\eta \neq 0$), it follows from the structure of $\alpha_{\xi\eta}(z)$ described in the previous section. This linear property of the first order approximation yields

$$u_1(x, y, z) = u_{2D}(x, z) + g(x, y, z), \tag{7.7}$$

where $u_{2D}(x, z)$ and $g(x, y, z)$ correspond to $B_{2D}(x)$ and $G(x, y)$, respectively. Here, $u_{2D}(x, z)$ is the first-order component of the velocity calculated by $B_{2D}(x)$ in accordance with formulas of Sect. 5. Hence, Eq. (7.6) can be used to define an implicit function $\zeta = \zeta(x, y)$,

$$\frac{1}{b} + \zeta\left(\frac{\partial u_{2D}}{\partial z}(x, 0) + \frac{\partial g}{\partial z}(x, y, 0)\right) = 0, \tag{7.8}$$

where $G(x, y)$ is assumed to be sufficiently smooth so that $g(x, y, z)$ and $\frac{\partial g}{\partial z}(x, y, z)$ can be represented by their Fourier series. The minimal positive value of η (for fixed values of x and y) is the critical $\varepsilon_e^{(3D)}$ for which regions arise where the flow is opposite to the bulk flow.

According to Subsect. 5.1, there exists a minimal positive $\varepsilon_e^{(2D)}$ such that

$$\frac{1}{b} + \varepsilon_e^{(2D)} \frac{\partial u_{2D}}{\partial z}(x_e, 0) = 0 \tag{7.9}$$

with some x_e. Substitute $x = x_e$ into (7.8), eliminate $\frac{\partial u_{2D}}{\partial z}(x_e, 0)$ from (7.8), (7.9) and calculate

$$\zeta(x_e, y) = \frac{1}{\frac{1}{\varepsilon_e^{(2D)}} - b\frac{\partial g}{\partial z}(x_e, y, 0)}. \tag{7.10}$$

The function $G(x, y)$ from (7.4) does not contain the zero-th term in its Fourier expansion in y. Hence, the function $g(x, y, z)$ constructed by $G(x, y)$ has the same property. Therefore, the zero-th term in the Fourier expansion of $b\frac{\partial g}{\partial z}(x, y, 0)$ vanishes and it can be written as

$$\int_{-\pi}^{\pi} b\frac{\partial g}{\partial z}(x, y, 0)dy = 0, \quad -\pi \leqslant x \leqslant \pi. \tag{7.11}$$

The latter equality implies that $b\frac{\partial g}{\partial z}(x, y, 0)$ for any fixed x can take negative, zero and positive values for some $y \in [-\pi,\pi]$. This implies that any sign from '' < '', '' = '', '' > '' between $\zeta(x_e, y)$ and $\varepsilon_e^{(2D)}$ takes place for any fixed $x_e \in S_{2D}$ and appropriate $y \in [-\pi, \pi]$. This implies

$$\varepsilon_e^{(3D)} = \min_{x,y} \zeta(x, y) \leq \min_{y} \zeta(x_e, y) < \varepsilon_e^{(2D)}. \tag{7.12}$$

This yields the following

Theorem. *For a given value of $\mathcal{R}e$, in any 3D channel, the critical value of $\varepsilon_e^{(3D)}$ when eddies start, is always less than the critical value $\varepsilon_e^{(2D)}$ for the corresponding 2D channel.*

The equality $\varepsilon_e^{(3D)} = \varepsilon_e^{(2D)}$ is possible if and only if $b\frac{\partial q}{\partial z}(x,y,0)dy \equiv 0 \Leftrightarrow G(x,y) \equiv 0$, i.e., when the 3D channel degenerates into a 2D channel. We emphasize that this assertion has been rigorously justified for sufficiently small ε. This theorem is analogous to Squire's theorem for the stability theory in time ([22], [23]) which states that if a 3D mode is unstable, a 2D mode is unstable at a lower $\mathcal{R}e$.

In order to illustrate these derivations, let us consider the case where $B(x, y)$ is given by (compare to (7.4))

$$B(x,y) = B_{2D}(x) + G(y). \tag{7.13}$$

Equation (7.7) becomes

$$u_1(x,y,z) = u_{2D}(x,z) + g(y,z), \tag{7.14}$$

where

$$g(y,z) = -2\sum_{\eta=1}^{\infty} B_{0\eta}\frac{\sinh\eta(b-z)}{\sinh\eta b}\cos\eta y. \tag{7.15}$$

Here, $B_{0\eta}$ are coefficients of the Fourier series of $G(y)$,

$$G(y) = 2\sum_{\eta=1}^{\infty} B_{0\eta}\cos\eta y.$$

Equation (6.12) was used to deduce (7.15). Calculation of $\frac{\partial q}{\partial z}(y,z)$ from (7.15) yields (compare to (7.10))

$$\eta(x,y) = \left(\frac{1}{\varepsilon_{2D}(x)} + 2b\sum_{\eta=1}^{\infty}\eta B_{0\eta}\coth\eta b\cos\eta y\right)^{-1}. \tag{7.16}$$

The difference between $\varepsilon(x, y)$ and $\varepsilon_{2D}(x)$ can also be estimated from (7.16). It is interesting to note that for channels (7.13), this difference does not depend on $\mathcal{R}e$. Moreover, this difference can be significant for non-smooth functions $G(y)$ (see Subsect. 5.2).

8 Symbolic and numerical computations

In Sect. 2, the full Navier–Stokes equations (2.6) with the boundary conditions (2.7) are reduced to a cascade of linear boundary value problems. The n-th solution $\mathbf{u}_n$ satisfies the linear equations (2.11) with the boundary conditions (2.15).

In Sect. 3, each boundary value problem (2.11), (2.15) is reduced to the non–local problem which is solved in Sect. 4.1 in closed form. In 2D channels, the components of the velocity u_n and w_n are given by (3.1), where $\alpha_\xi^{(n)}(z)$ and $\gamma_\xi^{(n)}(z)$ have the form (4.14). At each step n of the cascade, the constants C_1, C_2 and the function $f(z)$ have to be determined. The constants C_1, C_2 are given by (4.9), where $\Delta^{(\xi\eta)}$ is the same at any step, but D_1 and D_2 from (4.8) depend on $f(z)$ via (4.5) and on $\mathbf{H}_n(x, y)$. These functions $f(z)$ and $\mathbf{H}_n(x, y)$ change at each step of the cascade, since they depend on the previous approximations (see (2.16), (3.11) and (2.12)). Though all modes are separated in (3.1) at each step n, the functions $\mathbf{F}_n$ and $\mathbf{H}_n$ are constructed by modes produced by all modes of the previous steps as detailed by (2.12) and (2.16). The construction of $\mathbf{F}_n$ and $\mathbf{H}_n$ by converting all modes from the previous steps and their repartition onto new modes (3.1) is the most expensive part of the algorithm because the number of modes increases exponentially with n. Moreover, the frequency ξ is multiplied by $\mathcal{R}e$ (see (4.3) and other formulas). Hence, for large n, one can obtain

expressions involving Airy's functions with large ξ is $\xi\mathcal{R}e$ even for moderate $\mathcal{R}e$. Thus, a large number of frequencies in $B(x)$, large n or large $\mathcal{R}e$ yield the same numerical difficulties.

In order to improve the computations, numerically satisfactory pairs of fundamental solutions of Airy's equation and integral are used [18]. Symbolic–numerical computations were performed for $B(x)$ containing few modes with the precision $O(\varepsilon^4)$ for $\mathcal{R}e$ not exceeding 100 and ε less than 1. Actually, the Reynolds number can be taken very large $(\mathcal{R}e \sim 1000)$. The program is written in Mathematica©.

In the following subsections, the velocity is derived in the channel bounded by the surfaces

$$z = b, \quad z = -b\varepsilon\cos x, \tag{8.1}$$

i.e., $B_1 = B_{-1} = -\frac{1}{2}, B_\xi = 0$ $(\xi = \pm 2, \pm 3, \ldots)$. For such a wavy wall, the supremum of ε given by (4.18) is reduced to

$$\varepsilon_c = \mathcal{R}e^{-\frac{1}{2}}. \tag{8.2}$$

Therefore, the critical wall oscillations are of the usual order of the thickness of the boundary layer [22] though there is no boundary layer properly speaking in this paper.

8.1 Analytical formulas in the first order approximation

The first order approximation is discussed separately since analytical formulas can be obtained for an arbitrary channel. The formulas (5.7) imply that

$$\begin{aligned} u_1(x,z) &= \alpha_1^{(1)}(z)e^{ix} + \alpha_{-1}^{(1)}(z)e^{-ix}, \\ w_1(x,z) &= \gamma_1^{(1)}(z)e^{ix} + \gamma_{-1}^{(1)}(z)e^{-ix}. \end{aligned} \tag{8.3}$$

In this example, Eq. (5.9) becomes

$$\frac{1}{b} + (P(\mathcal{R}e)\cos x + Q(\mathcal{R}e)\sin x)\varepsilon = 0, \tag{8.4}$$

where the real values $P(\mathcal{R}e)$ and $Q(\mathcal{R}e)$ are defined by

$$\begin{aligned} P(\mathcal{R}e) &= 2Re\Big(\alpha_1^{(1)\prime}(0)\Big), \\ Q(\mathcal{R}e) &= -2Im\Big(\alpha_1^{(1)\prime}(0)\Big), \end{aligned} \tag{8.5}$$

$$\alpha_1^{(1)\prime}(0) = \frac{2}{\Delta^{(1)}}\int_0^b (\mathrm{Ai}[Z_1(0)]\mathrm{Bi}[Z_1(\tau)) - \mathrm{Bi}[Z_1(0)]\mathrm{Ai}[Z_1(\tau)))\sinh\tau\, d\tau. \tag{8.6}$$

Here, the relation $\alpha_{-1}(z) = \overline{\alpha_1(z)}$ is used (see 3.5). Direct calculations show that always $P(\mathcal{R}e) < 0$ and $Q(\mathcal{R}e) > 0$, except

$$Q(0) = 0. \tag{8.7}$$

Consider (8.4) as an equation in x. Introduce the value

$$x_0 = \arcsin\frac{Q(\mathcal{R}e)}{2b\sqrt{P(\mathcal{R}e)^2 + Q(\mathcal{R}e)^2}} \tag{8.8}$$

which belongs to the segment [0, π /2). Then, Eq. (8.4) becomes

$$\cos(x + x_0) = \frac{1}{b\varepsilon\sqrt{P(\mathcal{R}e)^2 + Q(\mathcal{R}e)^2}}. \tag{8.9}$$

This equation has a solution x if and only if $\varepsilon \geq \varepsilon_e$, where

$$\varepsilon_e = \frac{1}{b\sqrt{P(\mathcal{R}e)^2 + Q(\mathcal{R}e)^2}}. \tag{8.10}$$

Hence, for $0 \leq \varepsilon \leq \varepsilon_e$, there is no eddy. An eddy starts at $\varepsilon = \varepsilon_e$ given by (8.10). For $\varepsilon > \varepsilon_e$, separation and detachment points exist in the representative cell at $x = x_e$ given by (8.9),

$$x_e = -x_0 \pm \text{arc cos}\frac{1}{\text{b}\varepsilon\sqrt{\text{P}(\mathcal{R}\text{e})^2 + \text{Q}(\mathcal{R}\text{e})^2}}. \tag{8.11}$$

Equation (8.8) and the properties of the functions $P(\mathcal{R}e)$ and $Q(\mathcal{R}e)$ imply that $x_0 = 0$ only for $\mathcal{R}e = 0$. Therefore, an eddy arises at the lowest point of the channel $(0, -b\varepsilon)$ only for the Stokes (linear) equations. For positive $\mathcal{R}e$, the value x_0 is always positive. Hence, in this case, the geometrical symmetry is disturbed and an eddy always arises upstream of the lowest point.

Figures illustrating formulas (8.10)–(8.11) will be provided in Sect. 8.3 with a better precision in ε.

8.2 Asymptotic analysis for large Reynolds numbers

In the present section, the asymptotic behavior of ε_e is deduced from (8.10) for large $\mathcal{R}e$. The main difficulty is to estimate the integrals (8.6). For definiteness, the case $b = 1$ is studied. Hereafter, in this section, $\mathcal{R}e$ is assumed to be large. Consider one of the integrals

$$J(\mathcal{R}e) = \int_0^1 \text{Ai}[Z_1(\zeta)]e^{\zeta}d\zeta. \tag{8.12}$$

It follows from (4.15) that

$$Z_1(\zeta) \sim -i\zeta\mathcal{R}e^{1/3}. \tag{8.13}$$

For $Z \to \infty$ along the imaginary axis, Ai(Z) can be written as [18]

$$\text{Ai}[Z] = \frac{\exp(-\frac{2}{3}Z^{2/3})}{2\sqrt{\pi}Z^{1/4}}\left(\frac{1}{Z^{1/4}} + \text{O}\left(\frac{1}{Z^{5/4}}\right)\right). \tag{8.14}$$

The integral (8.12) is transformed into

$$J(\mathcal{R}e) \sim \int_0^1 \frac{(-1)^{1/8}\exp(\frac{2}{3}(-1)^{1/4}\sqrt{\mathcal{R}e}\zeta^{3/2})}{4\pi\mathcal{R}e^{1/6}\zeta^{1/2}}(1+\zeta)d\zeta, \tag{8.15}$$

where the formula $\exp\ \zeta \sim 1 + \zeta$ is used. All other polynomial approximations $\exp\ \zeta \sim 1 + \zeta + \frac{\zeta^2}{2!} + \cdots + \frac{\zeta^n}{n!}$ give the same order for $J(\mathcal{R}e)$, but with another factor which can be calculated. The roots of -1 are fixed in such a way that their positive arguments are minimal. For instance, $(-1)^{1/4} = e^{\pi\ i/4}$. The predominant terms in (8.15) imply that

$$J(\mathcal{R}e)\sim\mathcal{R}e^{-2/3}\exp\left(\frac{2}{3}(-1)^{1/4}\sqrt{\mathcal{R}e}\right). \tag{8.16}$$

The following formulas can be derived along similar lines,

$$\int_0^1 \mathrm{Ai}[Z_1(\zeta)]e^{-\zeta}d\zeta\sim\mathcal{R}e^{-2/3}\left(-3i+2^{2/3}3^{1/3}\Gamma(1/3)\mathcal{R}e^{1/3}\right),$$

$$\int_0^1 \mathrm{Ai}[Z_1(\zeta)]\sinh\zeta d\zeta\sim\mathcal{R}e^{-2/3}\exp\left(\frac{2}{3}(-1)^{1/4}\sqrt{\mathcal{R}e}\right),$$

$$\int_0^1 \mathrm{Bi}[Z_1(\zeta)]e^{\pm\zeta}d\zeta\sim\mathcal{R}e^{-2/3}\left(\mp3(-1)^{5/6}+2^{2/3}3^{1/3}\Gamma(1/3)\mathcal{R}e^{1/3}\right). \tag{8.17}$$

The asymptotics (8.16)–(8.17) can be substituted into (8.5)–(8.6),

$$P(\mathcal{R}e)+iQ(\mathcal{R}e)\sim-0.516541+(0.0406019-0.296042i)\mathcal{R}e^{1/3}. \tag{8.18}$$

Then, (8.10) yields the following asymptotic formulas:

$$\varepsilon_e\sim\mathcal{R}e^{-1/3} \tag{8.19}$$

and

$$\mathcal{R}e\sim\varepsilon^{-3}(1+0.516541\varepsilon)^3. \tag{8.20}$$

It follows from the convergence result that ε_e has to be smaller than the limit of convergence ε_c. This condition is fulfilled if in addition $ba_{\xi\eta}\sqrt{\xi^2+\eta^2}\sim\mathcal{R}e^{-1/6}$, where $a_{\xi\eta}$ is the amplitude of the Fourier series of $2B(x, y)$ with the mode (ξ, η) (see the end of the Appendix). This restriction is less strong than Sobey's restrictions for the Poiseuille flow (see [37], p. 227) $\varepsilon\sim\mathcal{R}e^{-1/3}$ and $\xi\sim\mathcal{R}e^{-1/7}$ in our notations.

8.3 Analytical formulas for higher order approximations

According to the algorithm described in Sect. 4.1 and 5, and to the remarks given at the beginning of Sect. 8, the results concerning higher order approximations for the channel are presented in this Subsection. The velocity is calculated up to $O(\varepsilon^5)$,

$$\mathbf{u}(x,z)=\left(\frac{z}{b},0\right)+\varepsilon\mathbf{u}_1(x,z)+\varepsilon^2\mathbf{u}_2(x,z)+\varepsilon^3\mathbf{u}(x,z)+\varepsilon^4\mathbf{u}_4(x,z)+O(\varepsilon^5). \tag{8.21}$$

The function $\mathbf{u}_1$ is given by (8.3) The functions $\mathbf{u}_j$ ($j = 2, 3, 4$) are also obtained in symbolic form. However, they are expressed by formulas which are so long that they cannot be given. The results presented in the following pictures are obtained by (8.21).

Some results are illustrated in Figs. 2–6. They are obtained with Padé approximations which allow in certain cases to continue the formulae for $\varepsilon > \varepsilon_c$ which here is estimated to be equal to 0.125 in application of (4.18). In Fig. 2, the streamlines are shown for $\mathcal{R}e = 64$ and $\varepsilon = 0.33$. The components of the velocity u and w for $\mathcal{R}e = 64$ and various ε are displayed in Fig. 3–Fig. 5 in the curvilinear coordinates $z(x, t) = b[t - \varepsilon\ (1 - t)\ \cos\ x]$ along the lines $t =$ constant. One can see here the change of the velocity with increasing ε. For $\varepsilon = 0.35$ the u-component becomes negative (see Fig. 4) and this corresponds to an eddy.

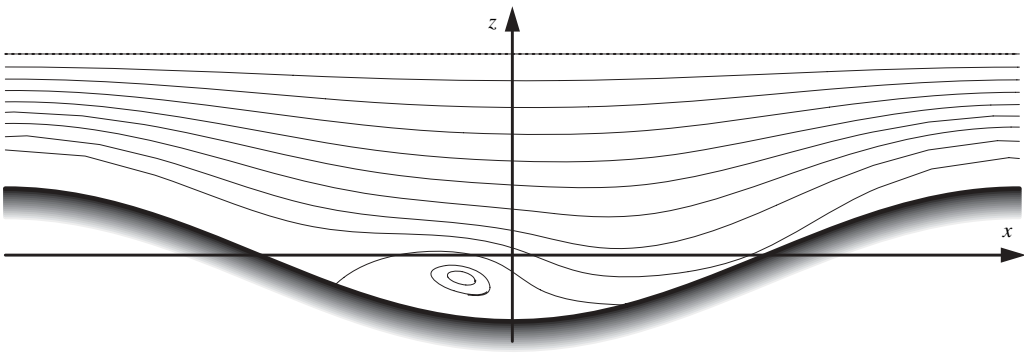

Fig. 2. Streamlines in the sinusoidal channel for $\mathcal{R}e = 64$ and $\varepsilon = 0.33$

An interesting pattern displayed in Fig. 6 was obtained for the streamlines for $\mathcal{R}e = 64$ and $\varepsilon = 0.45$. The eddy appears to be almost separated from the solid surface. Detailed computations show that the normal derivative of the tangent velocity is negative only on the very small part of the wall when $-0.15\pi < x < -0.24\pi$.

The analytical formulas (8.10) and (8.11) valid up to $O(\varepsilon^2)$ can be essentially improved by application of (8.21). In Fig. 7, the normal derivative at the wall of the tangential component of the velocity is displayed for $\mathcal{R}e = 64$ and various ε. One can observe in this picture the onset of eddies with the increase of ε. For $\varepsilon < 0.25$, the streamlines follow the wavy wall; for $0.25 < \varepsilon < 0.425$, one eddy arises; for $\varepsilon > 0.425$, a second small eddy arises near the point $x = \frac{\pi}{2}$.

In Fig. 8, the dependence of ε_e on $\mathcal{R}e$ is displayed. The solid line in Fig. 8 corresponds to the critical curve $\varepsilon_c(\mathcal{R}e)$ given by (8.2). Hence, points lying above $\varepsilon_c(\mathcal{R}e)$ should be considered with care despite the use of the Padé approximations. For small Reynolds number the calculations are consistent; for instance, the value $\varepsilon_e(\mathcal{R}e = 0) = 0.303094$ is obtained with an excellent precision already with the second order approximation. It should be noticed that precision problems arise for $\mathcal{R}e$ about 150; this corresponds precisely to the region where the condition (8.2) is not fulfilled at all.

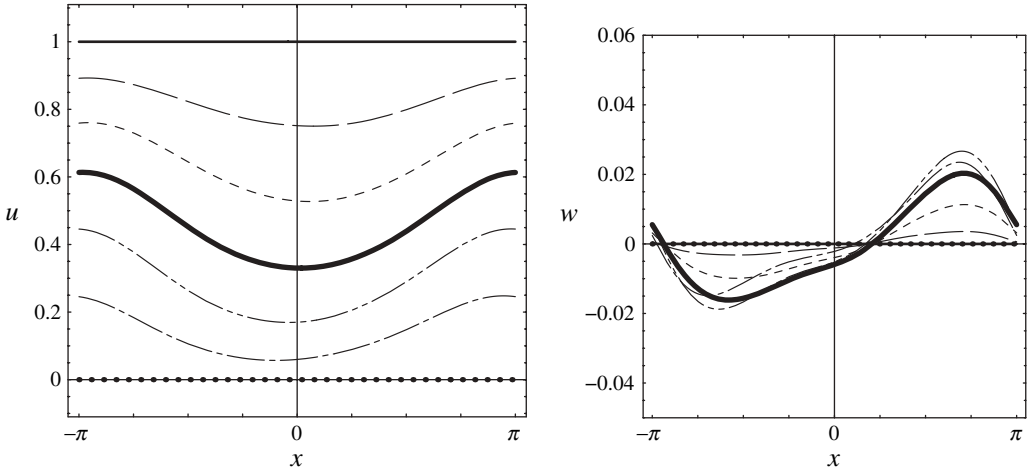

Fig. 3. The horizontal u and vertical w components of the velocity along the x-axis. $\mathcal{R}e = 64$, $\varepsilon = 0.2$. Data are for various depth levels: $t = 0$ (*dotted line*), $t = 0.17$ (*dash-dotted*), $t = 0.33$ (*dash-double-dotted*), $t = 0.5$ (*thick solid*), $t = 0.67$ (*short-dashed*), $t = 0.83$ (*long-dashed*) $t = 1$ (*solid*)

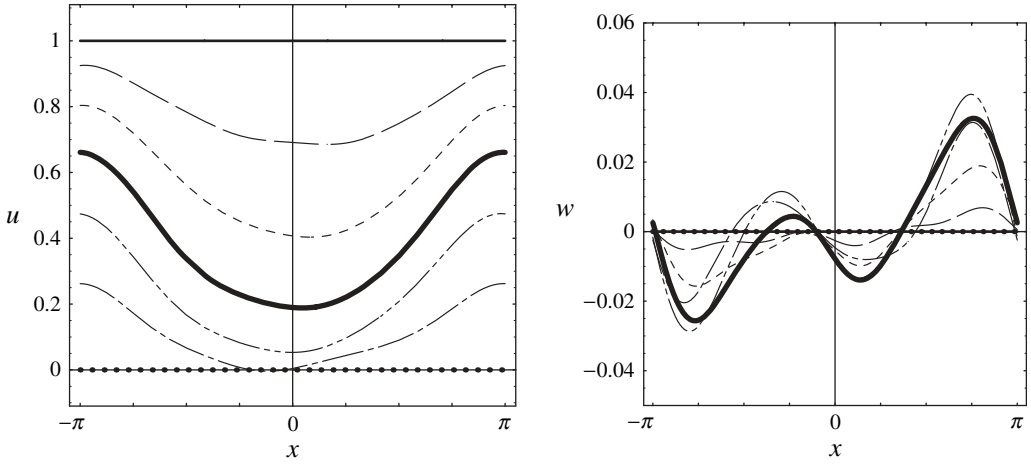

Fig. 4. The horizontal U_x and vertical U_z components of the velocity along the the x-axis. $\mathcal{R}e = 64$, $\varepsilon = 0.35$. Same convention as in Fig. 3

For larger values of $\mathcal{R}e$, the precision problems disappear and the curves for ε^3 and ε^4 which belong to the region $\varepsilon < \varepsilon_c(\mathcal{R}e)$, coincide for $\mathcal{R}e > 600$.

8.4 Drag on the top surface

The drag acting on the top wall is calculated by

$$\tau = \mu \int_{-\pi}^{\pi} \frac{\partial u}{\partial z}(x, b)dx. \tag{8.22}$$

In the present Section, the force is explicitly written up to $O(\varepsilon^4)$ for an arbitrary channel in analytic form. Numerical results are presented up to $O(\varepsilon^6)$ for a sinusoidal channel. When applied to 2D, (2.8) and (3.1) imply

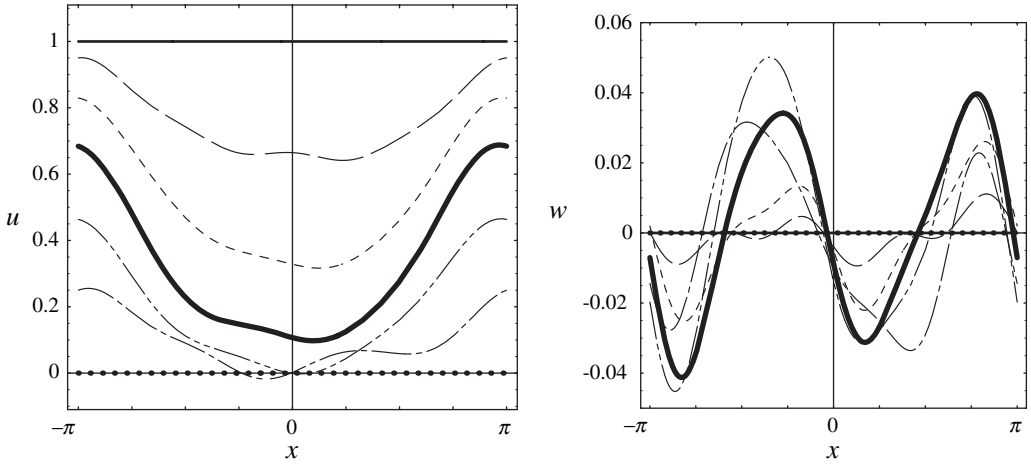

Fig. 5. The horizontal U_x and vertical U_z components of the velocity along the x-axis. $\mathcal{R}e = 64$, $\varepsilon = 0.45$. Same convention as in Fig. 3

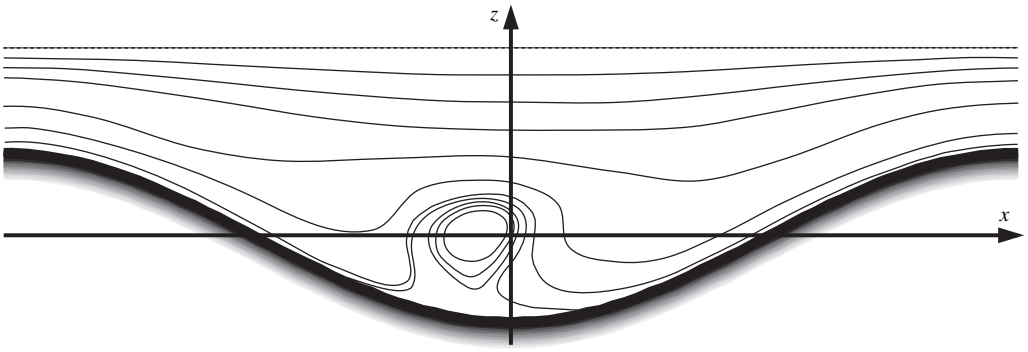

Fig. 6. An eddy almost strictly inside the channel; $\mathcal{R}e = 64$ and $\varepsilon = 0.45$

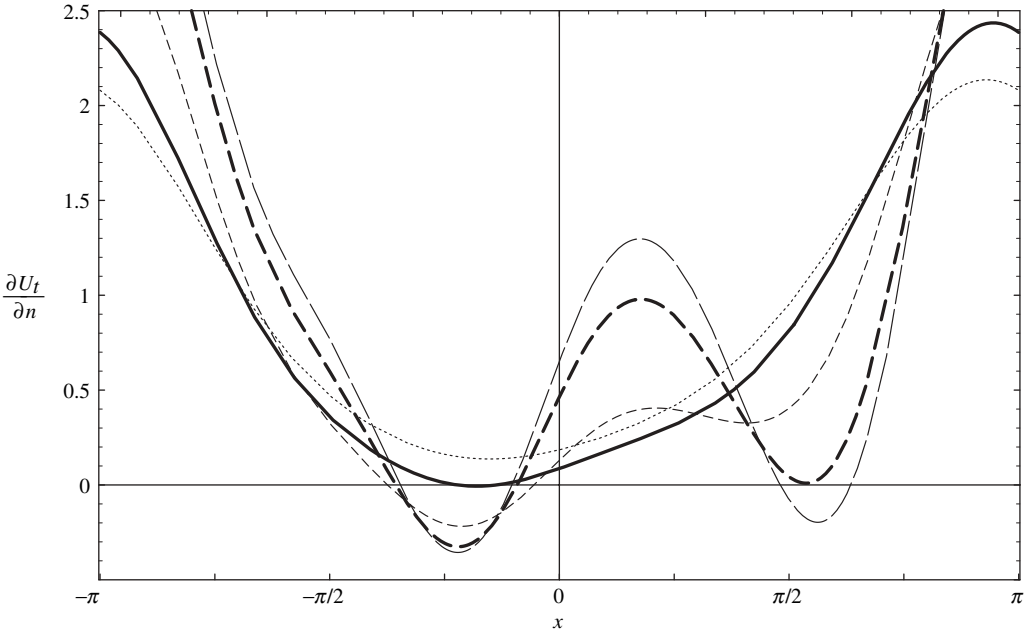

Fig. 7. The shear stress $\frac{\partial u_t}{\partial n}$ at the bottom wall as a function of the longitudinal coordinate s. $\mathcal{R}e = 64$. Data are for: $\varepsilon = 0.2$ (*dotted line*), 0.25 (*thick solid*), 0.35 (*dashed*), 0.425 (*thick dashed*), 0.45 (*long dashes*)

$$\frac{\partial u}{\partial z}(x,b) = \sum_{n=0}^{\infty} \varepsilon^n \sum_{\xi=-\infty}^{\infty} \alpha_{\xi}^{(n)'}(b) e^{i\xi x}. \tag{8.23}$$

Substitution of (8.23) into (8.22) yields

$$\tau = \mu \sum_{n=0}^{\infty} \alpha_{\xi}^{(n)'}(b) \varepsilon^n. \tag{8.24}$$

With the general algorithm described above to compute $\alpha_{\xi}^{(n)'}(b)$, we deduce the formula

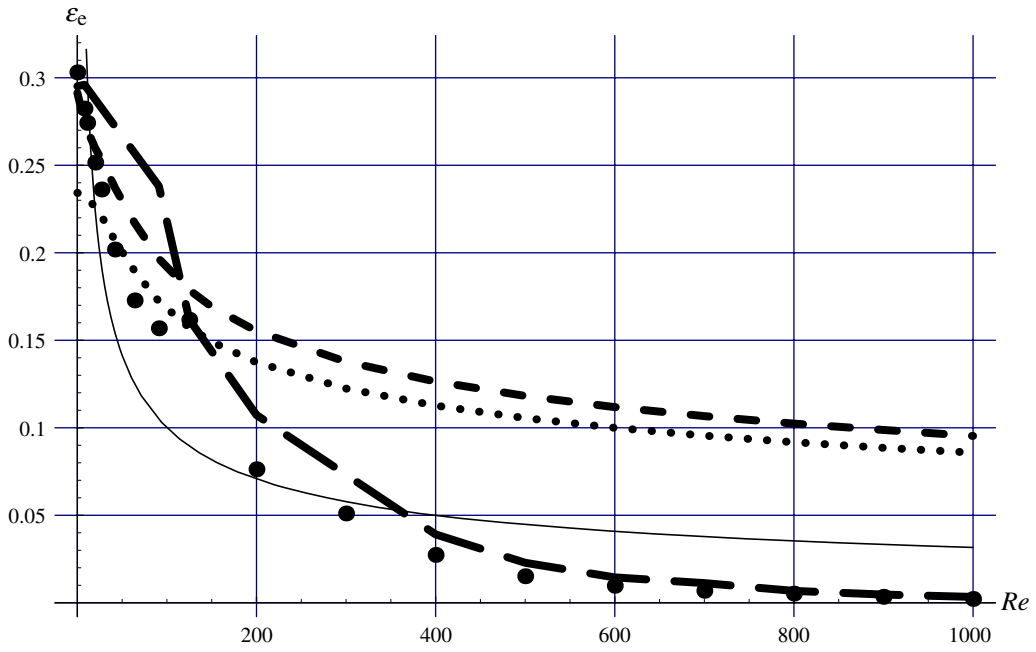

Fig. 8. ε_e as a function of $\mathcal{R}e$. Data are for: expansions to ε (*dotted line*), ε^2 (*dashed*), ε^3 (*long dashes*), ε^4 (*dots*). The solid line corresponds to the critical convergence value $\varepsilon_c = \frac{1}{\sqrt{\mathcal{R}e}}$

$$\tau = \frac{2\pi\mu}{b} - \frac{2\pi\mu}{b}\sum_{n=1}^{\infty}\varepsilon^n\left(\alpha_0^{(n)}(0) + \frac{2\mathcal{R}e}{b}\sum_{k=1}^{n-1}\sum_{\xi=1}^{\infty}\mathrm{Re}\left[\int_0^b \overline{\gamma_{1\xi}(\tau)}\alpha_{1\xi}(\tau)\mathrm{d}\tau\right]\right). \tag{8.25}$$

The ε^1-term of (8.25) is equal to zero, since $\alpha_0^{(1)}(0) = 0$. It follows from (5.4) with $B_0 = \int_{-\pi}^{\pi} B(x)dx = 0$ (compare to (2.2)).

Let us now calculate the ε^2-term of (8.25). First, $\alpha_0^{(2)}(0)$ is determined. (2.15) and (2.16) imply

$$u_2(x,0) = -bB(x)\frac{\partial u_1}{\partial z}(x,0). \tag{8.26}$$

The constant $\alpha_0^{(2)}(0)$ is the zero-th term in the Fourier expansion of (8.26). Hence,

$$\alpha_0^{(2)}(0) = -b\sum_{\xi=-\infty}^{\infty} B_\xi \alpha_{-\xi}^{(1)'}(0) = 2b\sum_{\xi=1}^{\infty}\mathrm{Re}\left[B_\xi\alpha_\xi^{(1)'}(0)\right], \tag{8.27}$$

where the relations $B_{-\xi} = \overline{B_\xi}$ and $\alpha_{-\xi} = \overline{\alpha_\xi}$ have been used (see (3.5)). Introduction of (5.4) yields the formula

$$\alpha_0^{(2)}(0) = -2b\sum_{\xi=1}^{\infty}|B_\xi|^2\mathrm{Im}\frac{(B^-(b) - B^+(b))\mathrm{Ai}[Z_\xi(\zeta)] + (A^+(b) - A^-(b))\mathrm{Ai}\left[e^{2\pi\mathrm{i}/3}Z_\xi(\zeta)\right]}{\Delta^{(\xi)}}, \tag{8.28}$$

where the notations (5.5), (5.6) are used.

Consider now the integral from (8.25) with $n = 2$ and $k = 1$. Application of the formulas (5.4) yields after tedious computations

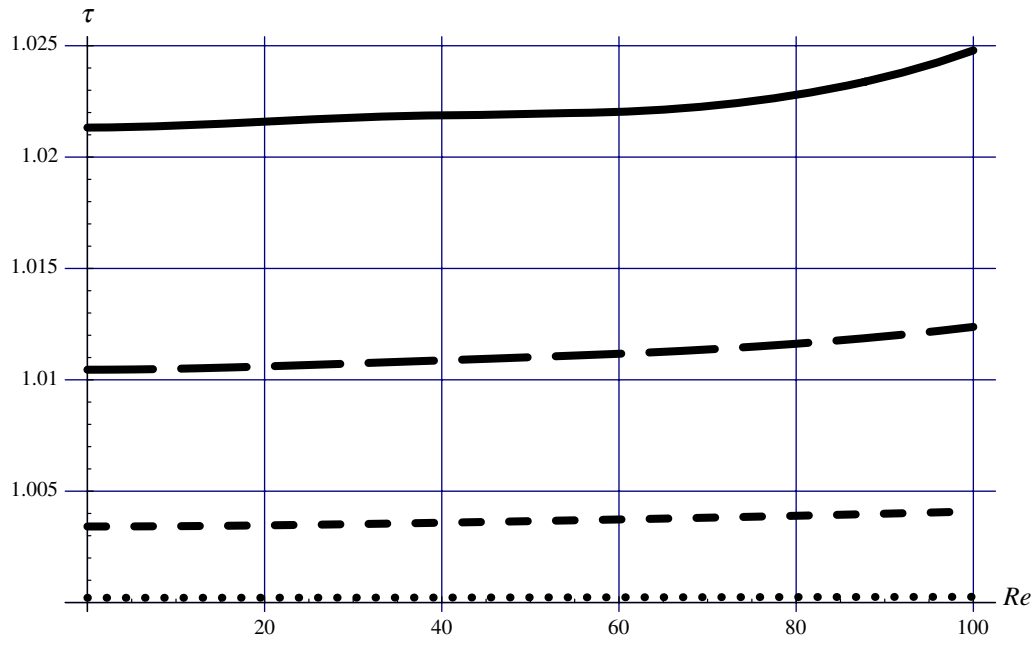

Fig. 9. Drag force τ calculated for: $\varepsilon = 0.01$ (*dotted*), $\varepsilon = 0.04$ (*short-dashed*), $\varepsilon = 0.07$ (*long-dashed*), $\varepsilon = 0.1$ (*solid*)

$$
\begin{aligned}
&\mathrm{Re}\left[\overline{\gamma_{1\xi}(z)}\alpha_{1\xi}(z)\right] \\
&= |B_\xi|^2\left(\mathrm{Im}\left[\frac{B^-(b)-B^+(b)}{\Delta}(A^+(z)-A^-(z))\right] + \mathrm{Im}\left[\frac{A^+(b)-A^-(b)}{\Delta}(B^+(z)-B^-(z))\right]\right. \\
&\quad + \frac{|B^-(b)-B^+(b)|^2}{2|\Delta|^2}\mathrm{Im}\left[\overline{A^+(z)}A^-(z)\right] + \frac{|A^+(b)-A^-(b)|^2}{2|\Delta|^2}\mathrm{Im}\left[\overline{B^+(z)}B^-(z)\right] \\
&\quad + \frac{1}{2|\Delta|^2}\mathrm{Im}\left[(B^-(b)-B^+(b))\overline{(A^+(b)-A^-(b))}\,\overline{B^+(z)}A^-(z)\right] \\
&\quad \left. + \frac{1}{2|\Delta|^2}\mathrm{Im}\left[\overline{(B^-(b)-B^+(b))}(A^+(b)-A^-(b))\overline{A^+(z)}B^-(z)\right]\right). \qquad (8.29)
\end{aligned}
$$

This function has to be integrated over (0,b) and the result has to be substituted into (8.25). The six corresponding double integrals are calculated numerically. This enables us to derive the following analytical approximate formulas for the drag force $\tau(\mathcal{R}e, \varepsilon)$ ($\mathcal{R}e$ is fixed in each formula):

$$\tau(0,\varepsilon) = 1 + 2.134439\varepsilon^2 - 0.202097\varepsilon^4, \quad \tau(8,\varepsilon) = 1 + 2.139841\varepsilon^2 - 0.165907\varepsilon^4,$$

$$\tau(64,\varepsilon) = 1 + 2.378837\varepsilon^2 - 18.189731\varepsilon^4 \approx \frac{1 + 10.0253\varepsilon^2}{1 + 7.64648\varepsilon^4}, \quad \tau(108.82,\varepsilon) = 1 + 2.616069\varepsilon^2,$$

$$\tau(125,\varepsilon) = 1. + 2.692240\varepsilon^2 + 19.937528\varepsilon^4 \approx \frac{1 - 4.71332\varepsilon^2}{1 - 7.40555\varepsilon^4}.$$

The Padé approximation [3] of the order (2, 2) for higher Reynolds numbers is used. One can see that the coefficient of ε^4 is equal to zero for $\mathcal{R}e = 108.82$. It is interesting to plot the data in various ways with the convergence criterion (8.2) in mind. For small values of ε, a wide range of $\mathcal{R}e$ can be studied. Results are displayed in Figs. 9 and 10 for $\varepsilon \leq 0.1$ and $\mathcal{R}e \leq 100$. When ε is very small,

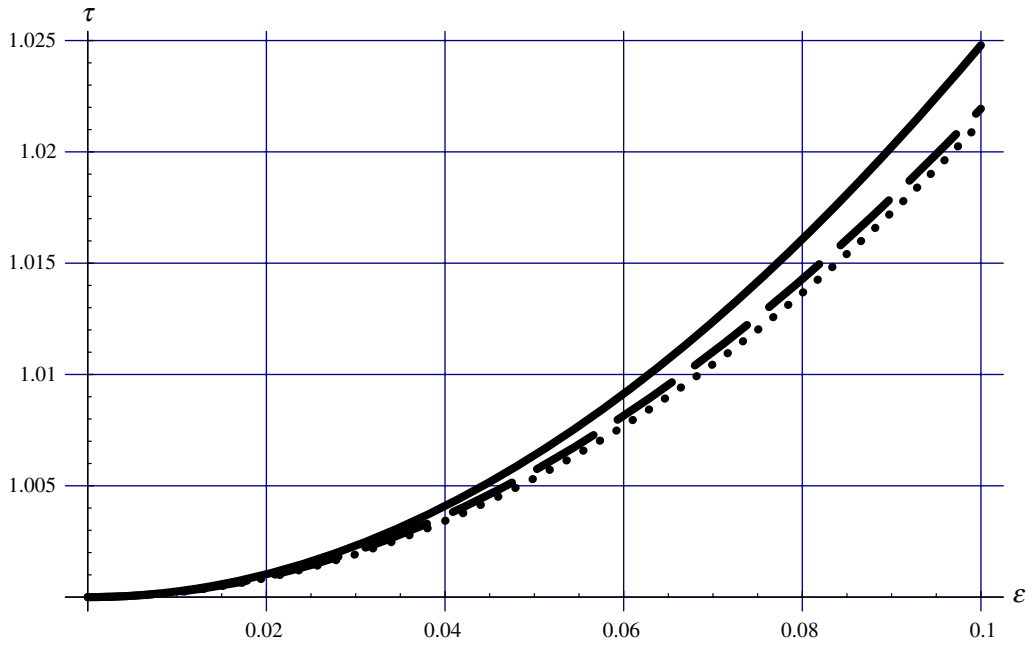

Fig. 10. Drag force $\tau(\varepsilon)$ calculated for: $\mathcal{R}e = 1$ (*dotted*), $\mathcal{R}e = 50$ (*dashed*), $\mathcal{R}e = 100$ (*solid*)

the wavy wall is almost flat and the influence of $\mathcal{R}e$ is very weak as seen in these two figures. It is only for values of ε larger than a few percents that this influence is significant.

Let us derive an expansion formula for the drag for values of ε and $\mathcal{R}e$ close to zero. Let $\tau(Re) = \tau_0 + \tau_1\ Re^d$. The function $\ln(\tau(Re) - \tau_0) = d\ \ln Re\ + \ln\tau_1$ is displayed in Fig. 11 for various values of ε. It shows that $d = 2$.

When ε is large, the possible range of $\mathcal{R}e$ is limited by (8.2). Figure 12 shows that for ε up to 0.3 the drags for $\mathcal{R}e$ equal to 1, 10 and 20 are practically equal.

9 Multiple solutions and ε_c

The critical convergence value ε_c given by (4.18) can be applied to the analysis of possible multiple solutions of the stationary problem (2.6)–(2.7) in the following way. It is known that the Couette flow for a straight channel ($\varepsilon = 0$) is stable [23], [6]; hence, the zero-th problem (2.6), (2.9) has the unique solution (2.10). It follows from the algorithm derived in Sect. 2–4.1 that each boundary value problem (2.11), (2.15)–(2.16) of the cascade has as many solutions as boundary value problems from the previous steps of the cascade. Hence, it has a unique solution as well as the problem (2.6), (2.7) due to (2.8). Therefore, it is justified that multiple solutions (equivalently bifurcation) can arise only for $\varepsilon > \varepsilon_c$, when the algorithm is not applied directly.

This idea is further developed for the 2D step channels described by

$$B(x) = \begin{cases} 1, & |x| < \pi h \\ -1, & \pi h < |x| < \pi. \end{cases} \tag{9.1}$$

For this channel, formula (4.18) becomes

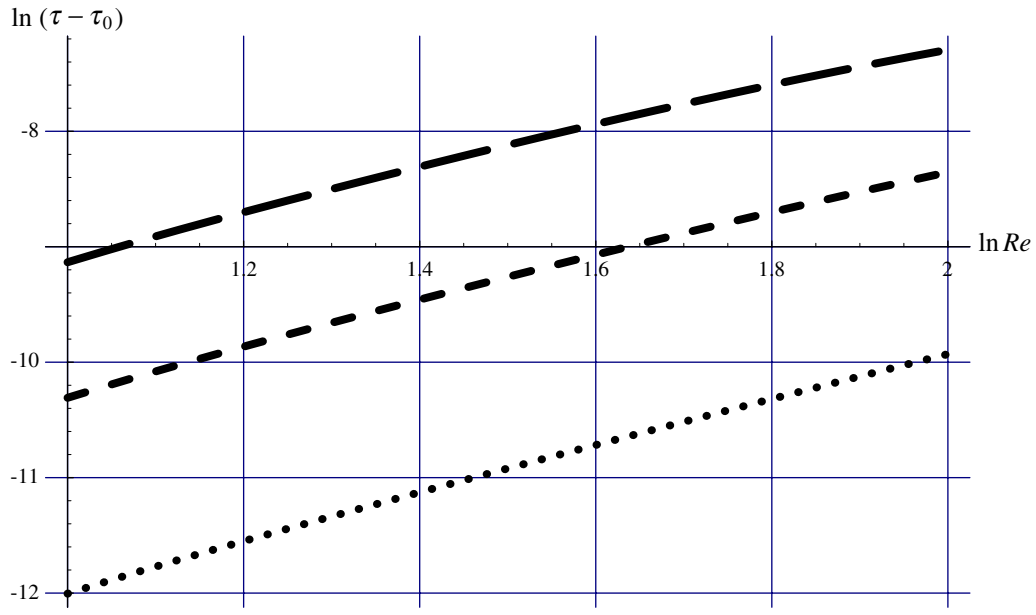

Fig. 11. $\ln(\tau(Re)-\tau_0)$ as a function of $\ln Re$. Data are for: $\varepsilon = 0.1$ (*dotted line*), 0.2 (*short-dashed*), 0.3 (*long-dashed*)

$$\varepsilon_c = \frac{\pi}{2b \sup_\xi A_\xi}, \tag{9.2}$$

where

$$A_\xi = |\sin \pi h\xi| \max\left(1, \sqrt{\frac{\xi}{\mathcal{R}e}}\right). \tag{9.3}$$

For definiteness, consider sufficiently large $\mathcal{R}e$ (it will follow from the forthcoming observations that $\mathcal{R}e > 1$). Then, (9.3) becomes

$$A_\xi = \frac{|\sin \pi h\xi|}{\sqrt{\xi}} \sqrt{\mathcal{R}e}. \tag{9.4}$$

Introduce the ratio of the height of the step, εb, to the distance between the cavities, $2\pi(1-h)$,

$$r = \frac{\varepsilon b}{2\pi(1-h)}. \tag{9.5}$$

Then, Eq. (9.2) can be written as

$$r_c = \frac{\varepsilon_c b}{2\pi(1-h)} = f(h)\frac{1}{\sqrt{\mathcal{R}e}}, \tag{9.6}$$

where

$$f(h) = \left(4(1-h) \sup_{\xi \in \mathbf{N}} \frac{|\sin \pi h\xi|}{\sqrt{\xi}}\right)^{-1}. \tag{9.7}$$

The critical value r_c corresponds to ε_c. The plot of the function $f(h)$ is presented in Fig. 13. The slope discontinuity is due to a change in the supremum of discrete values.

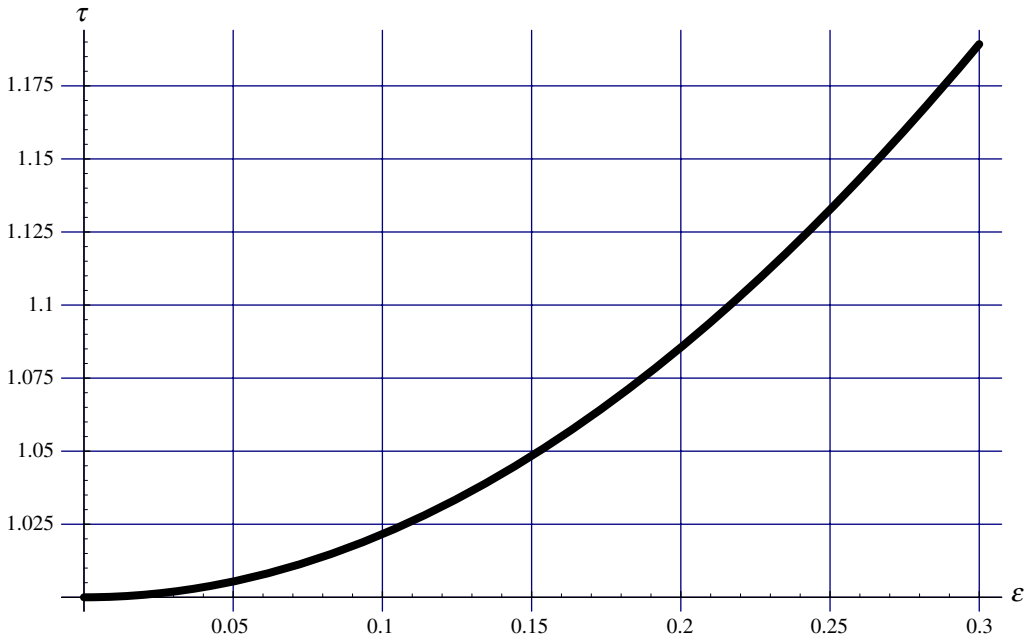

Fig. 12. The drag forces $\tau(\varepsilon)$ for $\mathcal{R}e = 1$, $\mathcal{R}e = 10$ and $\mathcal{R}e = 20$ are almost exactly superposed

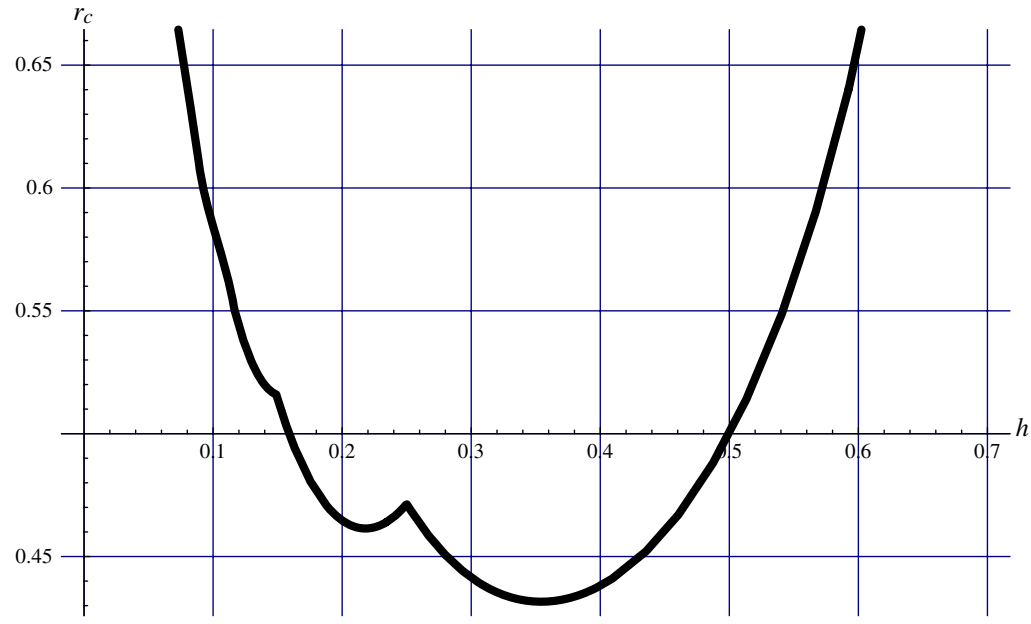

Fig. 13. The function $f(h)$ defined by Eq. (9.7)

Therefore, in the step channels, bifurcation can occur only if

$$r \geq r_c = f(h)\frac{1}{\sqrt{\mathcal{R}e}}. \tag{9.8}$$

10 Comparison with other results and discussion

Our results imply (see Sect. 8) that in horizontally symmetric channels an eddy arises at the bottom of the channel (a symmetry point of the channel) if and only if $\mathcal{R}e = 0$. For any $\mathcal{R}e > 0$, symmetry is disturbed and the separation point moves upstream; its location is a continuous function of $\mathcal{R}e$. This contradicts the numerical simulations of [14] where separation was supposed to be symmetrical for small $\mathcal{R}e$.

Formula (8.20) rigorously deduced for the Couette flow is surprisingly similar to the empirical Sobey's formula [36] for Poiseuille flow

$$\mathcal{R}e_e = 0.592\varepsilon_e^{-3}(1-\varepsilon_e)^2. \tag{10.1}$$

Application of higher order expansions in ε should yield higher order approximate analytical formulas for velocity, and for all detailed flow characteristics as done in [16]. However, numerical difficulties confine the application of our algorithm up to $O(\varepsilon^5)$. It is worth noting that analytical formulas for flow characteristics were given by previous authors in the framework of the linearized theory of boundary layer [31], i.e., up to $O(\varepsilon^1)$ in our notations. Therefore, even the case $O(\varepsilon^1)$ contains new results, since it is not limited by any geometrical restriction. Moreover, we stress that the dependence of the critical $\mathcal{R}e_e$ and ε_e is explicitly determined using the Fourier coefficients of $B(x, y)$ in symbolic form. Analytical formulas for the separation point x_e in 2D and separation set in 3D channels are deduced. For instance, the comparison of the separations in 2D and 3D channels implies that $\varepsilon_e^{(3D)}$ is always less than $\varepsilon_e^{(2D)}$. This assertion is analogous to the famous Squire's theorem from the classical stability theory [22], [23]. The obtained formulas are valid for geometries more general than in these works. Hovewer, a comparison is not always possible, since only the Couette problem is discussed here. Therefore, our results can be compared with [17], but not directly with Smith [29]–[33], Sobey [36], Zhou [45] who discussed Poiseuille flows.

A criterion of eddies in non–smooth channels is given in Subsection 5.2. This is not in agreement with Moffat's eddies [15] which do not arise for all angles. The reason of this discrepancy is due to different external flows.

Zhou et al. [45] did not observe eddies for $\mathcal{R}e = 0$ in a triangular channel. They calculated the velocity up to $O(\varepsilon^1)$ and took $\varepsilon = 0.1$. Actually, 10 modes in the Fourier series for the triangular channel were taken, i.e., flow in a smooth channel was investigated for which $\varepsilon_e > 0$. This is the reason why they did not observe any eddy. An eddy was obtained in [45] for $\mathcal{R}e = 4000$ in the same channel in agreement with our formula (8.19).

The calculations up to $O(\varepsilon^5)$ for the channel (8.1) give a detailed picture of the flow for various ε and $\mathcal{R}e$ (see Sect. 8). These analytical formulas are very convenient for fast numerical computations. This allows to describe systematically the complex behaviour of viscous fluids near the boundary and to easily find various unusual situations which can occur in a channel flow.

Appendix

Convergence of the algorithm

In [16], Poiseuille flows are investigated for the Stokes equations ($\mathcal{R}e = 0$) by the ε–expansion (2.8). In particular, the series (2.8) is shown to converge for

$$\varepsilon < \varepsilon_c = \left[b \sup_{\xi,\eta} a_{\xi,\eta} \sqrt{\xi^2 + \eta^2} \right]^{-1}, \tag{10.2}$$

where $a_{\xi,\eta}$ is the maximum modulus from four coefficients of $e^{\pm\xi\pm\eta}$ in the double Fourier series of $2B(x, y)$. Such formulas can be extended to non zero Reynolds numbers. It is the purpose of this Appendix to prove formula (4.18).

Let us fix a pair (ξ, η), i.e., a mode of the wavy channel and compare the orders of the terms in (3.6). The following relation can be easily proved by application of Leibnitz's rule by induction. The order of a function $f(z)$ and of its derivatives are related by $|f^{(n)}| \prec M^n|f|$, if $M = \sup_z |A(z)| > 1$ and all derivatives of $A(z) = f'(z)/f(z)$ are bounded. Then, the orders in (3.6) are obtained as

$$|\alpha''_{\xi\eta}| \prec \max(M^2|\alpha_{\xi\eta}|, M|\delta_{\xi\eta}|, M^2|\gamma_{\xi\eta}|), \tag{10.3.1}$$

$$|\beta''_{\xi\eta}(z)| \prec \max(M^2|\beta_{\xi\eta}|, M|\delta_{\xi\eta}|), \tag{10.3.2}$$

$$|\gamma''_{\xi\eta}| \prec \max(M^2|\gamma_{\xi\eta}|, |\delta'_{\xi\eta}|), \tag{10.3.3}$$

$$|\gamma'_{\xi\eta}| \prec \max(M|\alpha_{\xi\eta}|, M|\beta_{\xi\eta}|). \tag{10.3.4}$$

Let $|\alpha'_{\xi\eta}| \prec M_1|\alpha_{\xi\eta}|$, $|\beta'_{\xi\eta}| \prec M_2|\beta_{\xi\eta}|$, $|\gamma'_{\xi\eta}| \prec M_3|\gamma_{\xi\eta}|$, $|\delta'_{\xi\eta}| \prec M_4|\delta_{\xi\eta}|$. Based on (10.3) let us now prove that $M_j = M$ ($j = 1, 2, 3, 4$). We consider various relations between M_j and M. For definiteness, let us take

$$M_1 > M_2 > M_3 > M_4 > M. \tag{10.4}$$

The other cases can be considered in the same way. Relation (10.3.2) implies that $M_2^2|\beta_{\xi\eta}| \prec \max(M^2|\beta_{\xi\eta}|, M|\delta_{\xi\eta}|)$; therefore, by (10.4)

$$|\beta_{\xi\eta}| \prec MM_2^{-2}|\delta_{\xi\eta}|. \tag{10.5}$$

Along similar lines, the relation (10.3.3) yields

$$|\gamma_{\xi\eta}| \prec M_4M_3^{-2}|\delta_{\xi\eta}|. \tag{10.6}$$

Introduction of (10.5) and (10.6) into relation (10.3.4) yields

$$|\alpha_{\xi\eta}| \prec M_4M_3^{-1}M^{-1}|\delta_{\xi\eta}|, \tag{10.7}$$

since $M^2\, M_2^{-2} \; < M_4\, M_3^{-1}$. Substitution of (10.5)–(10.7) into the relation (10.3.1) shows that at least two of the following terms $M_1^2M_4M_3^{-1}M^{-1}|\delta_{\xi\eta}|, M|\delta_{\xi\eta}|, M^2M_4M_3^{-2}|\delta_{\xi\eta}|$ have the same order. Therefore, at least two of the three numbers $M_1^2\; M_4\; M_3^{-1}\; M^{-1}$, M, $M^2\; M_4\; M_3^{-2}$ must be equal in contradiction with the inequalities (10.4).

Therefore, $M_j = M$, i.e., $|\alpha_{\xi\eta}| \prec |\beta_{\xi\eta}| \prec |\gamma_{\xi\eta}| \prec M^{-1}|\delta_{\xi\eta}|$ and

$$|\alpha'_{\xi\eta}| \prec M|\alpha_{\xi\eta}|, |\beta'_{\xi\eta}| \prec M|\beta_{\xi\eta}|, |\gamma'_{\xi\eta}| \prec M|\gamma_{\xi\eta}|. \tag{10.8}$$

Let us now determine the order of $\mathbf{u}_n$ (2.11). For convenience, we introduce $\varepsilon' = b\ \varepsilon$ and find the critical value ε'_c. In this case, we can assume that $|B(x, y)| \prec 1$ and $b = 1$. We prove using induction on n that

$$\left| \frac{\partial^p \mathbf{u}_n}{\partial z^p}(x, y, z) \right| \prec \sup_{\xi\eta} a_{\xi\eta}^n M^{n+p-1}. \tag{10.9}$$

For $n = 1$ and $p = 0$, we have

$$|\mathbf{u}_1(x, y, 0)| = \left| -B(x, y) \frac{\partial \mathbf{u}_0}{\partial z}(x, y, 0) \right| \prec \sup_{\xi\eta} a_{\xi\eta}. \tag{10.10}$$

The estimation (10.10) on the boundary yields the same estimation as interior of the channel. Application of (10.8) p times to (10.10) implies

$$\left| \frac{\partial^p \mathbf{u}_1}{\partial z^p}(x, y, z) \right| \prec \sup_{\xi\eta} a_{\xi\eta} M^p \tag{10.11}$$

for $p = 0, 1, \ldots$ If by induction (10.9) is assumed to be valid for all $n = 0, 1, \ldots, m - 1$, it can be proved for $n = m$. (2.16) implies

$$|\mathbf{u}_m(x, y, 0)| \prec \sup_{\xi\eta} \sum_{k=1} \frac{a_{\xi\eta}^k}{k!} M^{m-1} \prec \sup_{\xi\eta} a_{\xi\eta}^n M^{m-1}. \tag{10.12}$$

Then, (10.8) implies again (10.9) for $n = m$. The conditions of the induction are fulfilled and (10.9) is proved.

Taking $p = 0$ in (10.9) and substituting it to (2.8), the series (2.8) is seen to converge if $\sup_{\xi\eta} a_{\xi\eta} M\varepsilon' < 1$. This implies (4.18).

In [16], the Padé approximations were applied to transform a polynomial in ε into a rational function; this extends the validity of the formulas for $\varepsilon \geq \varepsilon_c$. The Padé approximations are also used in the present paper with the same purpose. However, the Padé approximations degenerate into the first order approximation especially in the present paper. For instance, consider the formula (8.19). $\varepsilon_e \sim \mathcal{R}e^{-1/3}$. The value ε_e satisfies the restriction (4.18) if only $ba_{\xi\eta}\kappa \sim \mathcal{R}e^{-1/6}$.

References

[1] Adler, P. M.: Porous media. Geometry and transport. Butterworth-Heinemann 1992.

[2] Adler, P. M., Thovert, J.-F.: Fractures and fracture networks. Butterworth-Heinemann 1999.

[3] Baker, G. A.: Padé approximants. Cambridge: Cambridge University Press 1996.

[4] Carslaw, H. S.: An introduction to the theory of Fourier's series and integrals. New York: Dover 1950.

[5] Bowles, R. I., Davis, C., Smith, F. T.: On the spiking stages in deep transition and unsteady separation. J. Engng. Math. **45**, 227–245 (2003).

[6] Dyachenko, A. V., Shkalikov, A. A.: On a model problem for Orr–Sommerfeld equation with linear profile. Funkt Analiz i Prilozh **36**, 71–75, (russian) (2002).

[7] Floryan, J. M.: Vortex instability in a diverging-converging channel. J. Fluid Mech. **482**, 17–50 (2003).

[8] Hinch, E. J.: Perturbation methods. Cambridge: Cambridge University Press 1991.

[9] Kouakou, K. K. J., Lagrée, P.-Y.: Evolution of a model dune in a shear flow. Euro. J. Mech. B/Fluids **25**, 348–359 (2006).

[10] Lagrée, P.-Y., Lorthois, S.: The RNS/Prandtl equations and their link with other asymptotic descriptions. Application to the computation of the maximum value of the Wall Shear Stress in a pipe. Int. J. Engng. Sci. **43**, 352–378 (2005).

[11] Lagrée, P.-Y., Berger, E., Deverge, M., Vilain, C., Hirschberg, A.: Characterization of the pressure dropin a 2D symmetric pipe: some asymptotical, numerical and experimental comparisons. Z. Angew. Math. Mech. **85**, 141–146 (2005).

[12] Lagrée, P.-Y.: A triple deck model of ripple formation and evolution. Phys. Fluids **15**, 2355–2368 (2003).

[13] Landau, L. D., Lifshitz, E. M.: Theoretical physics. Moscow: Nauka 1986.

[14] Leneweit, G., Auerbach, D.: Detachment phenomena in low Reynolds number flows through sinusoidally constricted tubes. J. Fluid Mech. **387**, 129–150 (1999).

[15] Moffat, H. K.: Viscous and resistive eddies near a sharp corner. J. Fluid Mech. **18**, 1–18 (1964).

[16] Malevich, A. E., Mityushev, V. V., Adler, P. M.: Stokes flow through a channel with wavy walls. Acta Mech. **182**, 151–182 (2006).
[17] Munson, B. R., Rangwalla, A. A., Mann, J. A. III: Low Reynolds number circular Couette flow past a wavy wall. Phys. Fluids **28**, 2679–2686 (1985).
[18] Olver, F. W. J.: Asymptotic and special functions. NY: Academic Press 1974.
[19] Pozrikidis, C.: Creeping flow in two-dimensional channel. J. Fluid Mech. **180**, 495–514 (1987).
[20] Rothmayer, A. F., Smith, F. T.: Incompressible triple-deck theory, free interactions and breakaway separation. In Handbook on fluid mechanics, CRC Press 1998.
[21] Savin, D. J., Smith, F. T., Allen, T.: Transition of free disturbances in inflectional flow over an isolated surface roughness. Proc. R. Soc. Lond. A **455**, 491–541 (1999).
[22] Schlichting, H., Gersten, K.: Boundary-layer theory, 8th ed. Springer Verlag 2000. Corr. 2nd printing 2003.
[23] Schmid, P. J., Henningson, D. S.: Stability and transition in shear flows. Springer Verlag 2001.
[24] Scholle, M., Wierschem, A., Aksel, N.: Creeping films with vortices over strongly undulated channel. Acta Mech. **168**, 167–193 (2004).
[25] Scholle, M.: Creeping Couette flow over an undulated plate. Arch. Appl. Mech. **73**, 823–840 (2004).
[26] Scholle, M.: Hydrodynamical modelling of lubricant friction between rough surfaces. Tribol. Int. Available online (2006).
[27] Scholle, M., Rund, A., Aksel, N.: Drag reduction and improvement of material transport in creeping films. Arch. Appl. Mech. **75**, 93–112 (2006).
[28] Skjetne, E., Auriault, J.-L.: New insights on steady, non-linear flow in porous medium. Eur. J. Mech. B/Fluid **18**, 131–145 (1999).
[29] Smith, F. T.: Flow through constricted or dilated pipes and channels: Part 1. Quart. J. Mech. Appl. Math. **29**, 343–364 (1976).
[30] Smith, F. T.: Flow through constricted or dilated pipes and channels: Part 2. Quart. J. Mech. Appl. Math. **29**, 365–3376 (1976).
[31] Smith, F. T.: A two-dimensional boundary layer encountering a three-dimensional hump. J. Fluid Mech. **83**, 163–176 (1977).
[32] Smith, F. T.: Flow through symmetrically constricted tubes. J. Inst. Math. Appl. **31**, 473–479 (1978).
[33] Smith, F. T.: The separating flow through a severely constricted symmetric tube. J. Fluid Mech. **90**, 725–754 (1979).
[34] Smith, F. T., Walton, A. G.: Flow past a two- or three-dimensional steep-edged roughness. Proc. R. Soc. Lond. A **454**, 31–69 (1998).
[35] Smith, F. T.: On physical mechanism in two- and three-dimensional separations. Phil. Trans. R. Soc. Lond. A **358**, 3091–3111 (2000).
[36] Sobey, I. J.: On the flow through furrowed channel, Part 1: Calculated flow patterns. J. Fluid Mech. **96**, 1–26 (1980).
[37] Sobey, J.: Introduction to interactive boundary layer theory. Oxford University Press 2000.
[38] Stephanoff, K. D., Sobey, J., Bellhouse, J.: On flow through furrowed channels. Part 2. Observed flow patterns. J. Fluid Mech. **96**, 27–39 (1980).
[39] Stewartson, K.: Multistructured boundary layers on flat plates and related bodies. Adv. Appl. Mech. **14**, 145–239 (1974).
[40] Sychev, V. V.: On laminar separation, ''News of the USSR Academy of Sciences'', ''Fluid and Gas Mechanics'' (1972).
[41] Sychev, V. V., Ruban, A. I., Sychev, V. V., Korolev, G. L.: Asymptotic theory of separated flows. Cambridge: Cambridge University Press 1998.
[42] Sisavath, S., Al-Yaarubi, A., Pain, C. C., Zimmerman, R. W.: A simple model for deviations from the cubic law for a fracture undergoing dilatation or closure. Pure Appl. GeoPhys. **14**, 1009–1022 (2003).
[43] Wierschem, A., Scholle, M., Aksel, N.: Vortices in film flow over strongly undulated bottom profiles at low Reynolds numbers. Phys. Fluids **15**, 426–435 (2003).
[44] Wu, J. Z., Ma, H. Y., Zhou, M. D.: Vorticity and vortex dynamics. Springer-Verlag 2006.
[45] Zouh, H., Martinuzzi, J. C., Khayat, R. E., Straatman, A. G., Abu-Ramadan, E.: Influence of wall shape on vortex formation in modulated channel flow. Phys. Fluids **15**, 3114–3133 (2003).